AIMS Mathematics, 11(8): 26503–26537.
DOI: 10.3934/math.20261063
Received: 17 May 2026
Revised: 10 July 2026
Accepted: 05 August 2026
Published: 25 August 2026

https://www.aimspress.com/journal/Math

Research article

Fractional behaviors analysis and modelling using DRT

Jocelyn Sabatier* and Hamida Hallil

IMS laboratory, UMR 5218, University of Bordeaux, CNRS, Bordeaux INP, Talence 33400, France

*** Correspondence:** Email: Jocelyn.sabatier@u-bordeaux.fr; Tel: +33540008301; Fax: +33556371545.

Abstract: In this paper, we revisit the analysis and modelling of dynamical systems exhibiting apparent fractional behaviors using the framework of Distribution of Relaxation Times (DRT). We establish a formal mathematical equivalence between the DRT framework and diffusive representation. Moreover, we introduce a direct time-domain identification algorithm that extracts physically interpretable log-normal continuous distributions directly from raw input-output measurements, bypassing noisy frequency transforms. Through multiple engineering case studies (solar panels, epidemiological data, and tight sandstones), it is demonstrated, using the DRT concepts, that apparent fractional behaviors can often be accurately captured by compact, physically sound integer-order distributions, providing a robust structural diagnostic tool for fractional-order modelling.

Keywords: fractional behaviors; distribution of relaxation time; diffusive representation; fractional models; fractional calculus
Mathematics Subject Classification: 93B30, 93A30, 26A33

1. Introduction

The analysis of complex dynamical systems exhibiting memory effects, anomalous diffusion, and multi-scale relaxation mechanisms has intensified in recent years across fields such as physics, electrochemistry, porous media, and biological systems. Experimental evidence consistently shows that many real-world systems exhibit non-exponential relaxation, non-Fickian transport, or history-dependent responses that cannot be adequately described using classical first-order or low-order integer models. This has motivated the development of alternative mathematical frameworks capable of capturing long-range temporal correlations and broad relaxation spectra, such as generalized diffusion equations, distributed-parameter models, and spectral decompositions of

relaxation dynamics [1–3].

Among them, fractional-order models (or fractional calculus-based models) have gained popularity due to their ability to produce power-law memory kernels and to reproduce some experimentally observed phenomena. They have been widely used in electrochemistry, viscoelasticity, and biological modelling, in particular. However, it is now increasingly recognized that fractional models suffer from several critical limitations, including the following:

- **Lack of physical interpretability:** Fractional orders and fractional coefficients often lack clear physical meaning in many applications [4,5].
- **Structural non-uniqueness:** Different fractional models may fit the same data, and the observation of fractional behavior does not necessarily imply the need for a fractional model [6].
- **Lack of objectivity:** Two observers describing the same physical phenomenon with different time origins or two equivalent reference frames obtain different equations that cannot be transformed into one another [7].
- **Physical inconsistencies:** Physical analysis can invalidate the obtained model in the case of incommensurate orders [8] or may reveal unit inconsistencies in physical units [9].
- **Difficulties in numerical implementation and stability assessment:** This has led some authors to propose operators with non-singular kernels to replace the singular kernels used in the definition of fractional operators [10–12].
- **Fractional models implicitly impose infinite memory:** This complicates taking into account the initial conditions and the expression of the properties of these models (observability, controllability, etc.) and can make them inconsistent [13–15].
- **Inability to represent systems whose relaxation spectrum is not exactly a power law:** This is for instance the case for stretched exponential relaxation [16].
- **Absence of a canonical definition:** There are many non-equivalent definitions of a fractional derivative [17] that may lead to fundamentally different dynamics. As a result, system properties, model predictions, and parameter interpretations depend strongly on the chosen operator, raising concerns about physical consistency and model identifiability.

These limitations call for caution when using fractional models and suggest that:

- Preferentially consider other types of models if the aim is to study fractional behaviors (noting that fractional behaviors observed in real physical systems and fractional models are distinct concepts) such as those analyzed in [6].
- Use fractional models only when fully justified, i.e., when the fractional nature of the studied behaviors has been demonstrated.

However, this is not always the case in the literature, raising the following question: How do we determine whether a system to be modeled truly exhibits fractional behavior that requires the use of a model based on fractional calculus? This highlights the need for systematic criteria and analytical approaches to determine when the use of fractional calculus is justified, and when it should be avoided. Furthermore, given the limitations associated with fractional-order models, and the increasing availability of high-resolution time- and frequency-domain data, the community urgently needs robust, physically interpretable, and mathematically transparent alternatives.

Distribution of Relaxation Times (DRT) [18] and diffusive representations [19,20] offer such alternatives, each relying on the idea that the system response can be expressed as a continuous superposition of exponentially decaying modes. Although historically introduced in different research communities, their equivalence and modelling potential are often under-recognized. Furthermore,

despite their strong theoretical foundations, these tools remain under-used for analyzing whether a system genuinely exhibits fractional behavior or simply mimics it over a limited time or frequency range.

Conventionally, the DRT framework is utilized as a frequency-domain deconvolution tool for Electrochemical Impedance Spectroscopy data, relying heavily on advanced regularization techniques to solve the underlying ill-posed inverse problem [21,22]. Concurrently, the intrinsic link between the DRT and fractional calculus has emerged as a highly active research landscape. Researchers have extensively explored this relationship to evaluate the effective capacitance of Constant Phase Elements (CPE) [23] or to decipher the complex multiscale transient responses inherent to advanced electrochemical devices [24]. In transient time-domain investigations, the inclusion of a CPE in equivalent circuit models naturally governs relaxation dynamics via Mittag-Leffler functions [25,26]. However, these established frameworks remain predominantly tethered to frequency-domain data or analytical operator conversions. We distinguish this study by introducing a direct time-domain identification scheme that bypasses noisy integral transforms.

Objective of this paper is therefore fourfold:

1. To clarify the theoretical relationships between DRT, diffusive representation, and infinite-state formulations, showing that they constitute different expressions of the same underlying spectral decomposition framework.
2. To demonstrate that many behaviors, often interpreted as fractional, can be rigorously analyzed and disambiguated using DRT, thus preventing incorrect physical interpretations.
3. To show how DRT-based methods enable direct time-domain modelling from experimental data without explicitly identifying an impulse response or a transfer function.
4. To illustrate, through examples from the literature and electrochemical applications, how DRT-derived kernels can be used to construct accurate and physically meaningful models, providing an alternative to fractional-order formulations.

By establishing rigorous connections between these representations and by demonstrating their practical modelling implications, the paper aims to promote the use of DRT and diffusive representations as credible, interpretable, and numerically tractable alternatives to fractional-order models.

General notation note: Throughout this paper, all parameters and variables are assumed to be real-valued unless explicitly stated otherwise. In particular, the Laplace variable $s \in C$, the frequencies variable $\omega \in R_+$, the relaxation time $\tau \in R_+$, and all model coefficients (gain, time constants, exponents) are real. The distribution kernels $G(\tau)$ and $g(\tau)$ are real-valued positive functions on $\tau \in R_+$.

2. DRT, diffusive representation and infinite-state systems

2.1. Distribution of relaxation time (DRT)

The concept of DRTs is largely linked to electrochemistry and the modelling of dielectric relaxation processes. DRT originated from the need to represent the frequency response of complex materials (dispersive capacitances, dielectrics, porous electrodes, etc.) via a superposition of elementary RC responses [27]. It is defined by the following integral

$$H(j\omega) = \int_0^\infty \frac{G(\tau)}{1 + j\omega\tau}\, d\tau \qquad\qquad \omega \in \mathbb{R}_+^*, \tag{1}$$

in which j denotes the imaginary unit ($j = \sqrt{-1}$) and where the function $G(\tau) \in \mathbb{R}_+^*$ characterises

the distribution of relaxation times.

The first explicit integral formulation of DRT, which generalizes the Cole–Cole model [28], appeared in the work of Fuoss and Kirkwood in the 1940s [29]. They introduced an integral representation of complex permittivity, expressed as an integral over a relaxation time distribution, which is a direct generalization of the Debye model [30] (model with a single relaxation time). However, as heavily emphasized in the literature, the Fuoss-Kirkwood relation suffers from inherent ambiguities and rigid, limited behavioral flexibility when capturing highly asymmetric or non-ideal multiscale dynamics [31]. To overcome these structural limitations, DRT is used with highly adaptable continuous kernels, namely the log-normal, asymmetric log-normal, and modulated log-normal distributions (see Section 3.4 and Appendix). These mathematical structures provide the necessary degrees of freedom to fit non-ideal power-law behaviors without inheriting the rigid mathematical constraints of classical relations.

The DRT concept was later further developed in the 1970s–1980s within Electrochemical Impedance Spectroscopy (EIS), notably by Macdonald and colleagues. In [32], the DRT approach was explicitly introduced to interpret complex electrochemical responses, while [33] presents its theoretical development and applications to electrochemical materials.

If $h(t)$ denotes the impulse response of a system whose frequency response is given by relation (1), function $h(t)$ is defined by the relation

$$h(t) = \int_0^\infty G(\tau)\, e^{-t/\tau}\, \frac{d\tau}{\tau}, \qquad t \geq 0. \tag{2}$$

Using the change of variable $u = \frac{1}{\tau}$ and thus $d\tau = -\frac{1}{u^2} du$ relation (2) becomes,

$$h(t) = \int_0^\infty \frac{G\left(\frac{1}{u}\right)}{u^2}\, e^{-tu}\, du. \tag{3}$$

Let us define

$$\frac{G(1/u)}{u^2} = \varphi(u). \tag{4}$$

Thus, for $t \geq 0$,

$$h(t) = \mathcal{L}\{\varphi\}(s)|_{s=t}, \tag{5}$$

that is, the function $t \mapsto h(t)$ corresponds to the Laplace transform (in the variable u) of φ evaluated at $s = t$.

By applying the inverse Laplace transform,

$$\varphi(u) = \mathcal{L}^{-1}\{h\}(u) \tag{6}$$

(h being a function of s), and thus

$$\varphi(u) = \frac{1}{2\pi i} \int_{\gamma - j\infty}^{\gamma + j\infty} e^{su}\, h(s)\, ds, \tag{7}$$

where γ is chosen within the convergence domain of the integral. By replacing u by $1/\tau$ with $\tau > 0$ and using relation (4), then $\varphi(1/\tau) = G(\tau)\,\tau^2$ and thus an expression of the kernel $G(\tau)$ in (1) can be derived by

$$G(\tau) = \frac{1}{\tau^2}\,\mathcal{L}^{-1}\{h\}\left(\frac{1}{\tau}\right) = \frac{1}{2\pi j}\frac{1}{\tau^2}\int_{\gamma-j\infty}^{\gamma+j\infty} e^{\frac{s}{\tau}}\,h(s)\,ds. \tag{8}$$

Note that in relation (5), following Bernstein's theorem for completely monotonic functions, the complex Laplace variable s is evaluated strictly along the real axis, implying $Im(s) = 0$ when equated to the time variable t. Furthermore, in relation (8), the domain for the relaxation time is explicitly defined as $\tau > 0$, as $\tau = 0$ corresponds to an instantaneous boundary response and would introduce singularities into the integral kernel.

Taking into account the properties of the inverse Laplace transform, relation (8) is valid if the impulse response $h(t)$ is causal, exhibits bounded exponential growth ($\exists\ M > 0, b > 0$ such that $|h(t)| \leq Me^{bt}$ and locally integrable. Moreover, according to Bernstein's theorem, if $h(t)$ is completely monotonic ($(-1)^n\frac{d^n h}{dt^n}(t) \geq 0\ \ \forall n \geq 0\ \ t > 0$) then $G(\tau) \geq 0$, and the DRT is physically interpretable and well-defined as a positive density.

As an example, if $h(t)$ is the exponential function $h(t) = e^{-t/\tau_0},\ \tau_0 \in \mathbb{R}_+^*$, relation (7) gives

$$\varphi(u) = \frac{1}{2\pi i}\int_{\gamma-i\infty}^{\gamma+i\infty} e^{su}\,e^{-\frac{s}{\tau_0}}\,h(s)\,ds = \delta\left(u - \frac{1}{\tau_0}\right). \tag{9}$$

According to relation (4)

$$G\left(\frac{1}{u}\right) = u\delta\left(u - \frac{1}{\tau_0}\right) \tag{10}$$

and thus using the change of variable $\tau = 1/u$

$$G(\tau) = \tau_0\ \delta(\tau - \tau_0). \tag{11}$$

Now $h(t)$ is assumed not defined over a time $t = T \in \mathbb{R}_+^*$, and defined by:

$$h(t) = \begin{cases} 1 - e^{-\frac{t}{\tau_0}}, & 0 < t < T, \\ 0, & t > T. \end{cases} \tag{12}$$

The discontinuity at $t = T$ prevents $h(t)$ from being the Laplace transform of a regular function $\varphi(u)$ on $[0, \infty)$. In other words, there is no density $G(\tau)$ (ordinary, locally integrable, positive function) which exactly reproduces this $h(t)$ via relation (2).

Appendix A.1 presents the DRTs associated with several fractional operators and highlights that they correspond to a particular case of power-law DRT.

2.2. Diffusive representation and infinite-state representation

It was Montseny [19] who formally introduced the term and framework of diffusive representation in the modern sense of a long-memory operator (e.g., fractional differentiation, singular convolution), i.e., a continuous integral of exponentially decreasing states, interpreted as a diffusion system. This approach was subsequently formalized in the book [20], in which a linear operator with memory with input $u(t)$ and output $y(t)$ is defined through a diffusive state field $x(\xi, t)$ satisfying the following first-order differential equation

$$\frac{\partial x(\xi, t)}{\partial t} = -\xi x(\xi, t) + u(t) \qquad \xi \in \mathbb{R}_+. \tag{13}$$

Each function $x(\xi, t)$ thus corresponds to the state of a first-order system with decay rate ξ. To ensure mathematical rigor and eliminate boundary contradictions at the origin, the continuous analysis is formulated for $t > 0$, assuming that the system is strictly at rest prior to excitation (namely, zero initial conditions: $x(\xi, 0) = 0$ at $t = 0^-$). Under this assumption, the time-domain equivalence formulations remain perfectly valid.

The representation output is obtained by integrating these states with weight $\mu(\xi)$, $\mu(\xi)$ being the relaxation density (or spectral distribution), with the relation

$$y(t) = \int_{\Omega} \mu(\xi) x(\xi, t) d\xi. \tag{14}$$

In relation (14), Ω is a general spectral domain. In the particular case $\Omega = R_+$ and if the input $u(t)$ is a Dirac function $u(t) = \delta(t)$, the output $y(t)$ is an impulse response $h(t)$ that can be written as

$$h(t) = \int_0^{\infty} e^{-\xi t}\ \mu(\xi)\, d\xi, \tag{15}$$

as the solution of Eq (13) is $x(\xi, t) = e^{-\xi t}$, $\xi \in \mathbb{R}_+$ (without considering initial conditions). The use of a one-sided integral in (15) is justified by causality: the impulse response is zero for $t < 0$.

Relation (15) is thus a particular case of diffusive representation, in which the memory kernel is expressed as a continuous superposition of elementary exponential modes as with DRT. In this particular case ($\Omega = \mathbb{R}_+$), an analytical link can even be established between DRT and diffusive representation. Applying the Fourier transform to (15) yields to

$$H(j\omega) = \int_0^{\infty} \frac{\mu(\xi)}{\xi + j\omega}\ d\xi. \tag{16}$$

Note that the Fourier transform of a causal signal is defined as a two-sided integral, but since the impulse response is zero for $t < 0$ ($h(t) = 0$ for $t < 0$), it reduces to a one-sided Laplace transform evaluated at $s = j\omega$.

Using the change of variable $\xi = 1/\tau$ and thus $d\xi = -1/\tau^2\, d\tau$ in relation (16) leads to

$$H(j\omega) = -\int_{\infty}^{0} \frac{1}{\tau^2} \frac{\mu(1/\tau)}{1/\tau + j\omega} d\theta\ = \int_0^{\infty} \frac{1/\tau\, \mu(1/\tau)}{1 + j\tau\omega} d\tau \tag{17}$$

and a comparison of relation (17) with relation (1), demonstrates that the DRT is a particular case of diffusive representation in which the relaxation distribution function $G(\tau)$ is defined by the relation

$$G(\tau) = \frac{1}{\tau} \mu\left(\frac{1}{\tau}\right). \tag{18}$$

In some cases, notably for the classical Warburg cell with impulse response $h(t) = 1/\sqrt{\pi t}$, there is even equality of relations as

$$\mu(\xi) = \frac{1}{\pi\sqrt{\xi}} \qquad \text{and} \qquad G(\tau) = \frac{1}{\pi\sqrt{\tau}}. \tag{19}$$

Based on the preceding developments, it can therefore be concluded that a DRT is a particular case of diffusive representation where diffusive states are Debye-type relaxations.

It must be noted that in equivalent circuit models, the presence of a Warburg cell or a Constant

Phase Element (CPE) (ideal modelling case) naturally leads to the appearance of Mittag-Leffler functions $E_\alpha(-t^\alpha)$ with real parameter $\alpha \in [0,1]$ when transforming the equations into the time domain, thus highlighting fractional relaxation dynamics. Under transient conditions, this fractional-order capacitor behavior maps onto a continuous power-law distribution of relaxation times $G(\tau)$, as shown by relation (19). By duality, a dispersive inductor can be represented through a continuous distribution of inductive relaxation rates. This yields a structurally analogous mathematical formulation where the elementary Debye-type kernel is adapted to capture high-frequency or inductive features rather than capacitive ones.

3. Fractional behavior analysis and modelling with DRT

3.1. An algorithm for DRT computation from input-output data

From the input signal $u(t)$ and the output signal $y(t)$ of a linear time-invariant system, a model based on the DRT can be formulated, without ever going through the impulse response $h(t)$ or the transfer function $H(s)$.

Since DRT enables the system impulse response $h(t)$ to be modeled as a weighted superposition of exponential responses as (see relation (2))

$$h(t) = \int_0^\infty G(\tau)\frac{1}{\tau}e^{-\frac{t}{\tau}}d\tau, \tag{20}$$

the system output can thus be defined by the double convolution:

$$y(t) = \int_0^\infty G\,(\tau)\left(\frac{1}{\tau}\int_0^t u\,(t-\vartheta)e^{-\vartheta/\tau}d\vartheta\right)d\tau \tag{21}$$

that can also be written as

$$y(t) = \int_0^\infty G\,(\tau)k(t,\tau)d\tau \tag{22}$$

with

$$k(t,\tau) = \frac{1}{\tau}\int_0^t u\,(t-\vartheta)e^{-\frac{\vartheta}{\tau}}d\vartheta. \tag{23}$$

It is therefore possible to construct an algorithm that directly approximates $G(\tau)$ from $u(t)$ and $y(t)$ using a discretization of variables t and τ. For each discrete value $t_n = nT_e$ $n \in N_+$ of t and $\tau_i \in [\tau_0..\tau_{N_\tau}]$ of τ, $T_e \in R_+^*$ being the sampling period, integral (22) can be approximated by the Riemann sum

$$y(t_n) = \sum_{i=1}^{N_\tau} \gamma(\tau_i)k(t_n,\tau_i)(\tau_i - \tau_{i-1}). \tag{24}$$

The coefficient $k(t_n,\tau_i)$ in relation (24) results from relation (23) and is defined by

$$k(t_n,\tau_i) = \frac{1}{\tau_i}\int_0^{t_n} u\,(t_n-\vartheta)e^{-\frac{\vartheta}{\tau_i}}d\vartheta, \tag{25}$$

an integral that can be approximated by the discrete convolution

$$k(t_n, \tau_i) \approx \frac{T_e}{\tau_i} \sum_{m=0}^{n} u(t_n - mT_e) e^{-\frac{mT_e}{\tau_i}}. \tag{26}$$

From relation (26) written for various time $t_n,\ n \in (1..N_t),\ N_t \in \mathbb{N}_+$, it is possible to write a relation of the form

$$Y = K\Gamma \text{ with } Y = \begin{bmatrix} y(t_1) \\ \vdots \\ y(t_n) \end{bmatrix} \text{ and } \Gamma = \begin{bmatrix} G(\tau_1) \\ \vdots \\ G(\tau_{N_\tau}) \end{bmatrix}. \tag{27}$$

An approximation of the weight function $G(\tau)$ can thus be obtained by minimizing the function (modelling error)

$$\|K\Gamma - Y\|_2^2. \tag{28}$$

Finding the vector Γ is an ill-posed inverse problem that can be solved using a Tikhonov regularisation [34] and by posing a regularised inverse optimization problem. The criterion (28) is therefore replaced by:

$$\|K\Gamma - Y\|_2^2 + \lambda \|L\Gamma\|_2^2, \tag{29}$$

where $\lambda \in \mathbb{R}_+^*$ is the regularisation parameter and L is a second difference matrix (tridiagonal matrix with the pattern [1, –2, 1]), used to penalise the curvature of $G(\tau)$. As

$$\|K\Gamma - Y\|_2^2 = [K\Gamma - Y]^T [K\Gamma - Y] \quad \text{and} \quad \lambda \|L\Gamma\|_2^2 = \left[\sqrt{\lambda} L\Gamma\right]^T \left[\sqrt{\lambda} L\Gamma\right], \tag{30}$$

relation (29) becomes

$$\begin{bmatrix} K\Gamma - Y \\ \sqrt{\lambda} L\Gamma \end{bmatrix}^T \begin{bmatrix} K\Gamma - Y \\ \sqrt{\lambda} L\Gamma \end{bmatrix} \text{ thus } \left\| \begin{bmatrix} K \\ \sqrt{\lambda} L \end{bmatrix} \Gamma - \begin{bmatrix} Y \\ 0 \end{bmatrix} \right\|_2^2. \tag{31}$$

3.2. Dynamical behavior analysis using DRT prior to fractional modelling

The use of fractional models to describe the behavior of dynamical systems from experimental data introduces additional challenges compared to classical integer-order models (manipulation of complex concepts, need for specific discretization/simulation methods, etc.).

Furthermore, as discussed in the introduction, these models present several limitations and may lead to misleading conclusions when used to infer the properties of the underlying physical system. Consequently, the use of fractional calculus and fractional calculus for modelling dynamic behaviors requires particular justification.

However, such justification is not always explicitly provided in the literature. As illustrated in this section through examples drawn from the literature, DRT can be used to establish criteria to clarify such situations.

3.2.1. A first analysis

A first analysis was done for the data presented in [35]. The goal is to model the dynamic behavior of a solar panel that links, as [35, Figure 10] shows, the current applied to the panel to the electrical

power produced by the panel. In the sequel and according to [35], the current is considered as the system input $u(t)$ and the power as the system output $y(t)$. These two signals are represented in Figure 1.

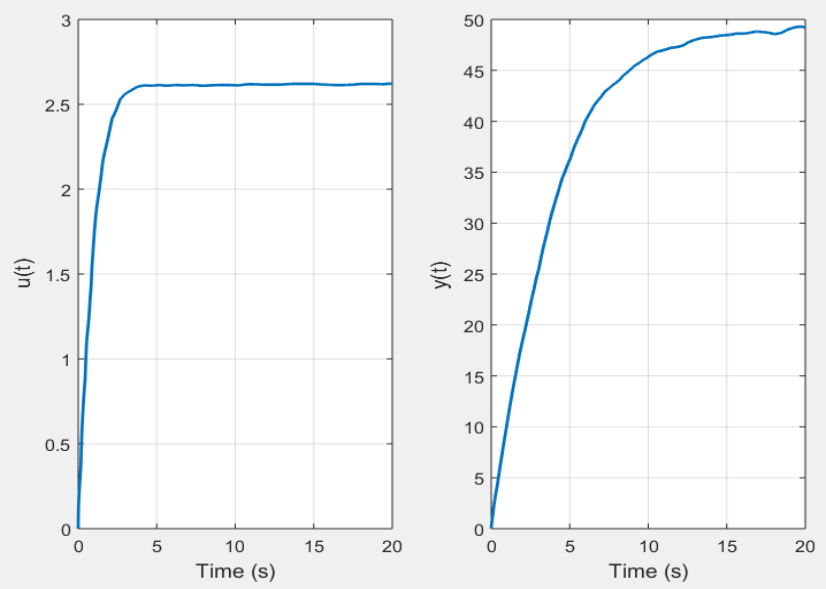

Figure 1. Input signal $u(t)$ (left) and output signal $y(t)$ (right) respectively current applied and power produced by the solar panel modelled in [35] with a fractional model.

In [35], the dynamic behavior of the system linking signals $u(t)$ and $y(t)$ is modeled by a fractional model. However, the following question arises: Is the use of this class of model and the constraints it imposes justified? To provide some answers, a DRT analysis is done. Using the algorithm presented in Section 3.1, the model

$$H(j\omega) = K_0 + \int_0^{\infty} \frac{G(\tau)}{1 + j\omega\tau}\, d\tau \qquad K_0 \in \mathbb{R} \tag{32}$$

is computed (algorithm adapted to include parameter K_0). Figure 2 shows the function $G(\tau)$ of the optimal model obtained, with the optimal value of K_0 being $K_0 = 3.254$. Figure 2 also compares the signal $y(t)$ and the response of obtained model $H(j\omega)$. It highlights that the function $G(\tau)$ and parameter K_0 permit an accurate fitting of signal $y(t)$. Figure 2 also shows that the DRT kernel $G(\tau)$ is concentrated around $\tau_0 = 3.5$ s. The narrowness of this peak (close to a Dirac function) indicates that a single exponential mode (i.e., a first-order system) is sufficient to capture the dynamics. Given relation (11), this suggests that modeling the system using a fractional order model is not justified and that a simple first-order model would be able to capture the input-output behavior of the system. To verify this assertion, we propose now to fit the system dynamic behavior with a model described by the transfer function

$$H_a(s) = K_0 + \frac{K_1}{\tau_1 s + 1} \qquad K_1 \in \mathbb{R}, \qquad \tau_1 \in \mathbb{R}_+^*. \tag{33}$$

Given the previous DRT analysis, $K_0 = 3.254$ is imposed in model (33). Parameters K_1 and τ_1 are computed using a nonlinear Levenberg-Marquardt optimization algorithm that minimizes the

quadratic error between signal $y(t)$ and the output of model (33) (the model input being $u(t)$). The values obtained are:

$$K_1 = 15.58 \qquad \text{and} \qquad \tau_1 = 3.484. \tag{34}$$

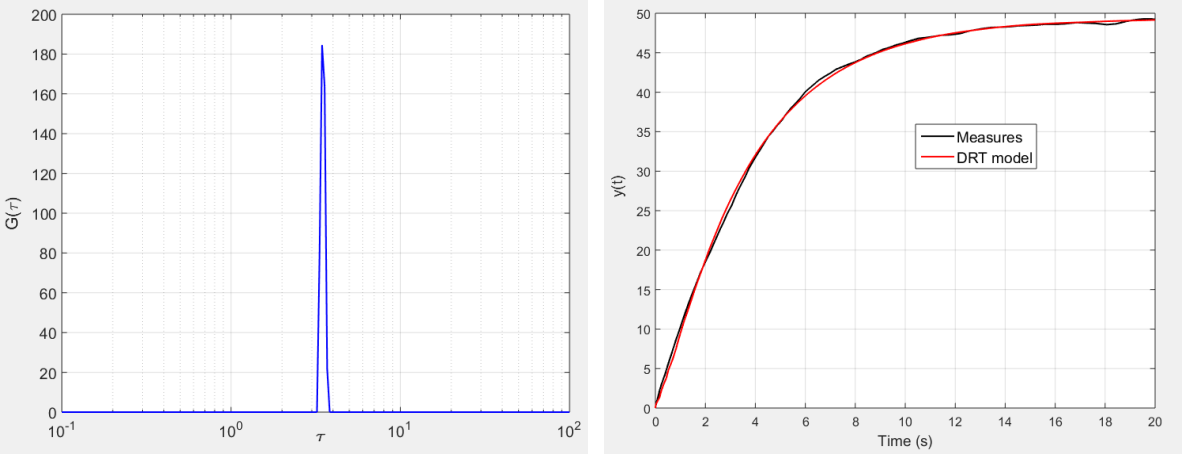

Figure 2. Function $G(\tau)$ obtained in model (32) (left) and comparison of the output signal $y(t)$ with the response of model (32).

The response of model (33) fitted with parameters (34) is compared in Figure 3 to the signal $y(t)$ and shows a very small error which is comparable to that of the fractional model.

It can thus be concluded that the system dynamic behavior can be captured by a first-order model and that a fractional model does not contribute much, as suggested by the shape of the function $G(\tau)$ resulting from the DRT modelling.

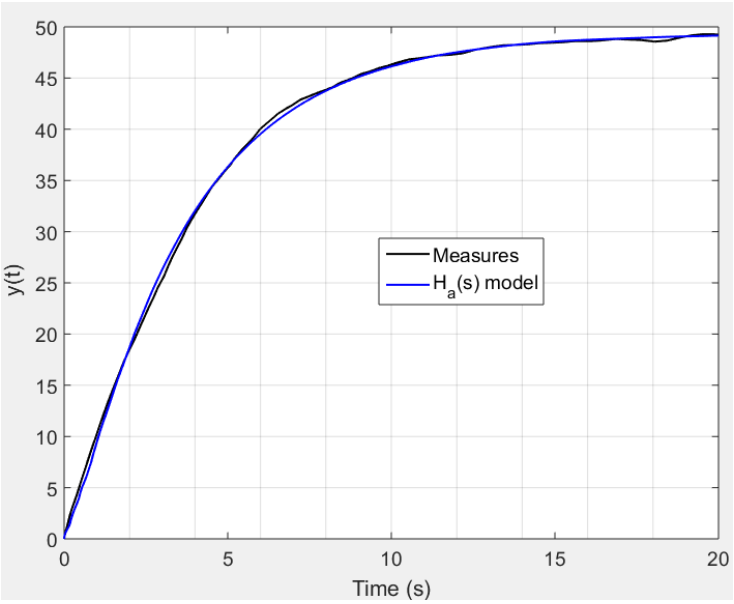

Figure 3. Comparison of the output signal $y(t)$ with the output of the model of the transfer function $H_a(s)$.

3.2.2. A second analysis

Fractional models have been widely used to model the kinetics of epidemics such as COVID-19 [36] or Ebola [37]. The data from [38] are analyzed in this section, particularly those in [38, Figure 11], as they can be considered a step response (the other data from this paper are similar). The data analyzed are public and can be found at:
https://www.data.gouv.fr/fr/datasets/donnees-relatives-a-lepidemie-decovid-19-en-france-vue-dense mble/.

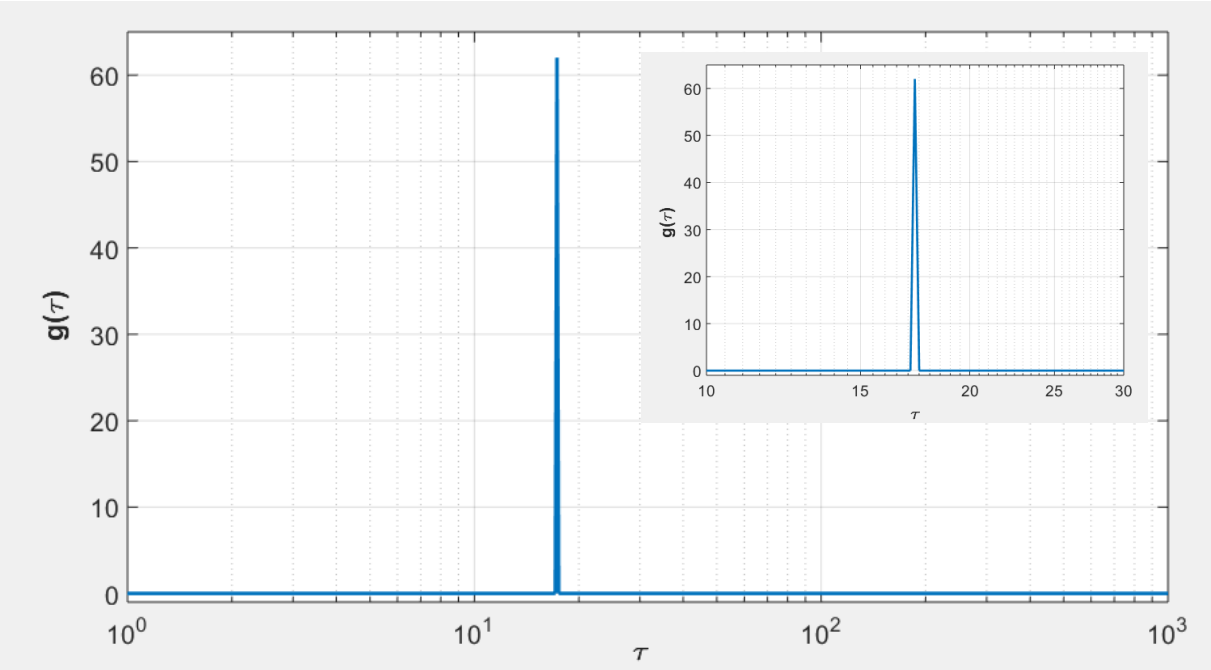

Figure 4. DRT corresponding to data of [38, Figure 11], viewed as a step response.

Using the algorithm described in Section 3.1, Figure 4 represents the DRT obtained on the data in [38, Figure 11].

The DRT in Figure 4 resembles a Dirac function and suggests that the system has first-order behavior. As illustrated in Figure 5, the response of [38, Figure 11] can be fitted with great precision with the function

$$Ke^{-\omega_0 t} + C_0, \qquad K \in \mathbb{R}, \qquad \omega_0 \in \mathbb{R}, \qquad C_0 \in \mathbb{R}. \tag{35}$$

This is also true for all the data analyzed in [10], as shown in Figure 5.

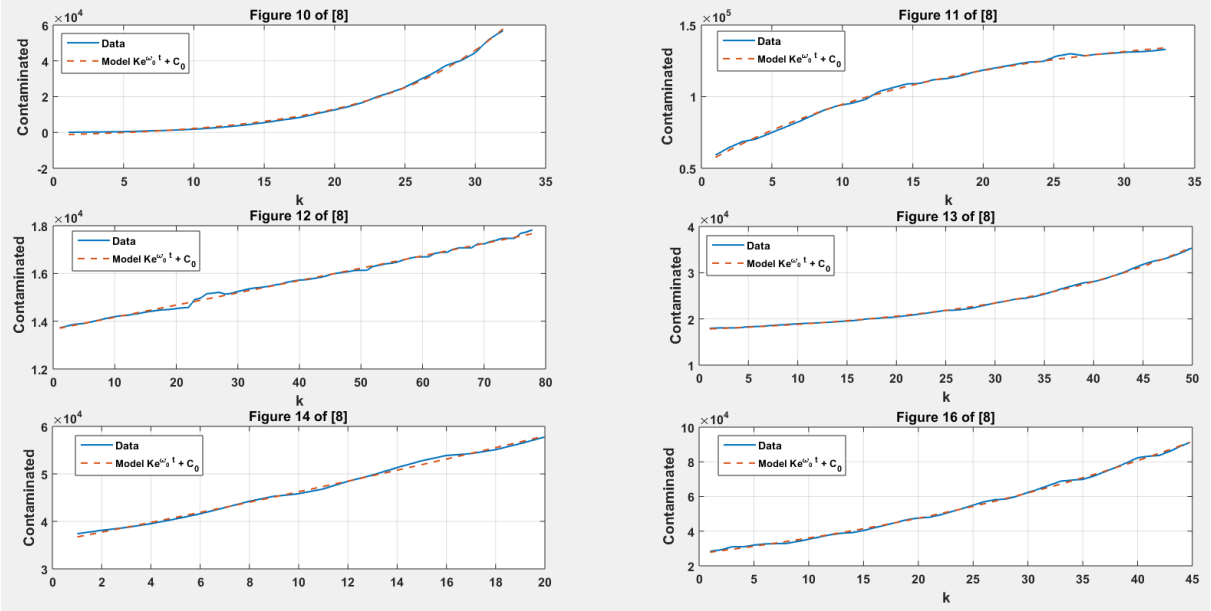

Figure 5. Fitting of the data analyzed in [38] with relation (35).

In [38], the authors chose to model the data with the function

$$A + Bt^n, \qquad n \in \mathbb{R}, \qquad A \in \mathbb{R}, \qquad B \in \mathbb{R}. \tag{36}$$

This is indeed a possibility, but the presence of a term in t^n does not justify the link with fractional calculus or fractional models as claimed in [38]. The integer nonlinear system

$$\frac{dy(t)}{dt} = nB^{(\frac{1}{n})}(y(t) - A)^{\frac{n-1}{n}} \qquad n \in \mathbb{R}. \tag{37}$$

also produces such trajectories.

The same type of analysis and questionable results are proposed in [39]. Moreover, contrary to what the authors claim in [40], model (36) does not provide a better prediction than the exponential model, since, as illustrated in Figure 6 with the data in [40, Figure 3], there is at least one exponential function that fits the entire measurement window (identification + prediction sections). This discrepancy may be attributed to limitations in the identification procedure used in [39,40], which may not have captured the appropriate exponential representation, suggesting that the identification approach used may not have been fully adapted to this type of data. The exponential function has a stronger growth rate than the polynomial function, and a parameter estimation error has thus a greater impact for longer time periods. The ability to fit the data with an exponential function is confirmed by the DRT presented in Figure 6.

A prior and more in-depth analysis of the measurements in [38–40] using tools such as DRT could help avoid such ambiguities.

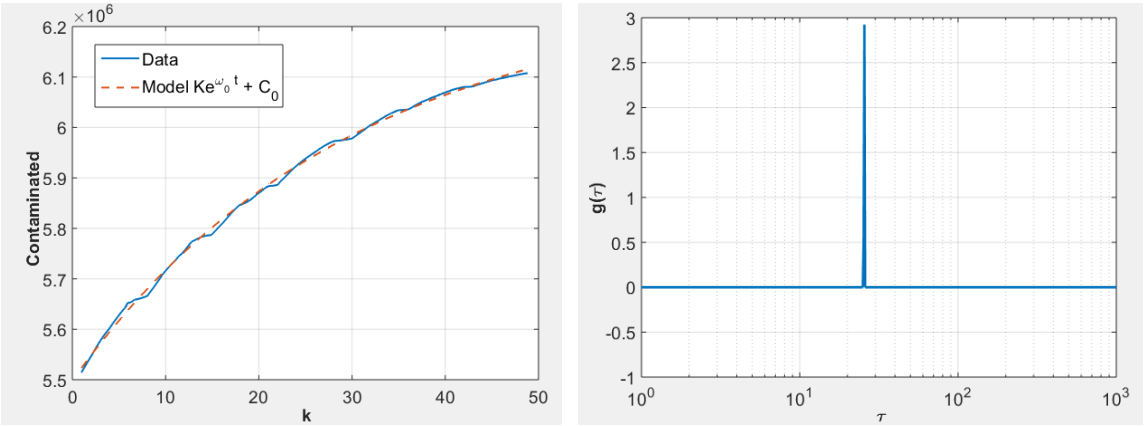

Figure 6. Fitting of data in [40, Figure 3] with relation (35) identification + prediction sections and DRT resulting from the data.

3.2.3. A third analysis

It is known that viscoelastic materials are sources of fractional behaviors. It is thus proposed in this section to work on the data presented in [41]. They correspond to the deformation of tight sandstone under axial stress. In [41], the time dependence of the creep compliance $J(t)$ is fitted by a fractional Maxwell model defined by

$$J(t) = \frac{1}{E_0} + \frac{1}{\eta^\alpha} \frac{t^\alpha}{\Gamma(1+\alpha)}, \tag{38}$$

where $E_0 \in \mathbb{R}_+^*$ is the elastic modulus of the Hooke spring, $\eta^\alpha \in \mathbb{R}_+^*$ is the generalized viscosity of the Scott Blair dashpot and $\alpha \in [0,1]$ is the fractional order. As shown in Figure 7 model (38) permits a nice fitting of the data of [41, Figure 3.b]. However, the need of such a model may be questioned. It is therefore relevant to examine whether a simpler model, such as those considered in the previous subsections, could provide an adequate description. To provide some answers, a DRT analysis of the data in Figure 7 was performed using the algorithm of Section 3.1. The response of the DRT model also appears in Figure 7, and is even closer to measurements than the fractional model.

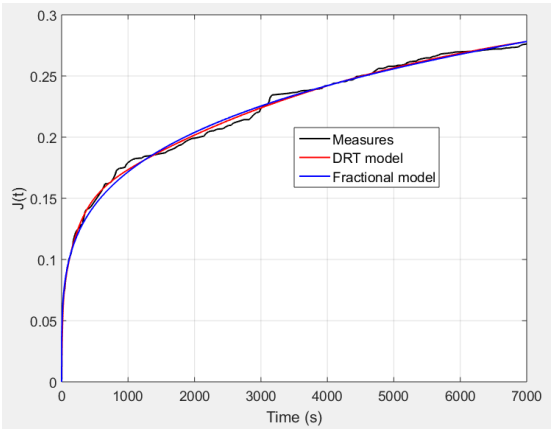

Figure 7. Fitting experimental deformation data of a tight sandstone sample under axial stress of 10 Mpa: measures presented in [41, Figure 3.b] (black), DRT model fitting (red),

fractional model fitting (blue).

The kernel $\tau G(\tau)$ produced by the algorithm of Section 3.1 on the measures of [41, Figure 3.b] is represented by Figure 8. This is compared to the same kernel for the function $\frac{1}{\eta^\alpha}\frac{t^\alpha}{\Gamma(1+\alpha)}$ in (37) that can be computed analytically [42] (see also the appendix) and that is defined by

$$\frac{1}{\eta^\alpha}\frac{sin(\alpha\pi)}{\pi}\tau^{1-\alpha}. \tag{39}$$

The shape of the DRT kernel in Figure 8 reveals a broad distribution of time constants, which justifies the use of a fractional model. However, the right panel shows that this continuous distribution can be approximated by a discrete sum of four exponentials, providing an integer-order alternative, namely a model of the form:

$$F(s) = \sum_{i=1}^{N} \frac{A_i}{\tau_i s + 1} \qquad \text{with} \qquad A_i > 0 \qquad \forall i. \tag{40}$$

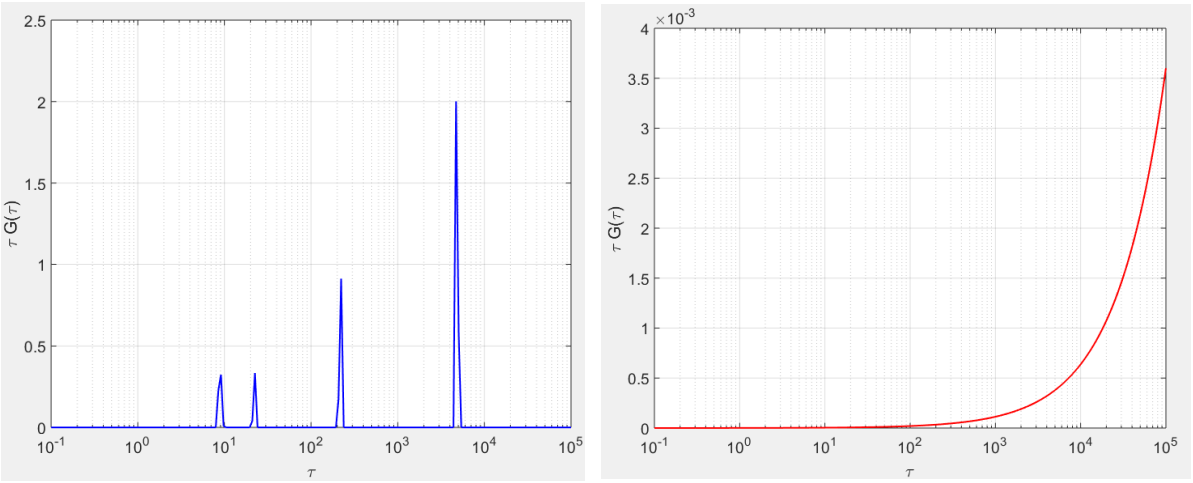

Figure 8. Comparison the kernel $\tau G(\tau)$ produced by the algorithm of Section 3.1 on the measures of [41, Figure 3.b] (left) and of the kernel given by relation (39).

To check if the model of the transfer function $F(s)$ is a good candidate to capture the experimental sandstone sample behavior, an optimization problem aiming at minimizing the error

$$\varepsilon = \sum_{k=1}^{N_t} \frac{\left(J(t_k) - \tilde{J}(t_k)\right)^2}{N_t} \tag{41}$$

is implemented, in which $\tilde{J}(t)$ denotes the step response of the model (40) and N_t is the number of samples of $\tilde{J}(t)$. This optimization problem is solved for several values of N (number of time constants if model $F(s)$). Table 1 gives the error values (41) after optimization for $N \in [2,6]$.

Table 1 shows that the smallest error value is obtained for $N = 4$. For this value the following results are obtained

$$A_1 = 3.8634 \times 10^{-2} \qquad \tau_1 = 8.9.$$

$$A_2 = 2.6029 \times 10^{-2} \qquad \tau_2 = 21.8.$$
$$A_3 = 7.5712 \times 10^{-2} \qquad \tau_3 = 218.7.$$
$$A_4 = 1.7922 \times 10^{-1} \qquad \tau_4 = 4780.6.$$

Table 1. Error values ε for various values of N.

N	2	3	4	5	6
ε	1.65898x10^{-5}	7.32205x10^{-6}	7.31381x10^{-6}	7.31847x10^{-6}	2.11901x10^{-5}

The obtained time constants are close to the one shown in Figure 8 on the left. The distribution of amplitudes associated with these time constants (values of A_i) also varies in proportions similar to those in Figure 8 on the left.

This analysis highlights the value of a DRT analysis. It reveals the distribution necessary to capture the dynamics of a system. In this example, the DRT analysis supports the use of fractional modelling over classical integer-order models. A fractional model with 3 parameters leads to a modelling that is as accurate as an integer model ($F(s)$ transfer function) with 8 parameters, as shown by Figure 9.

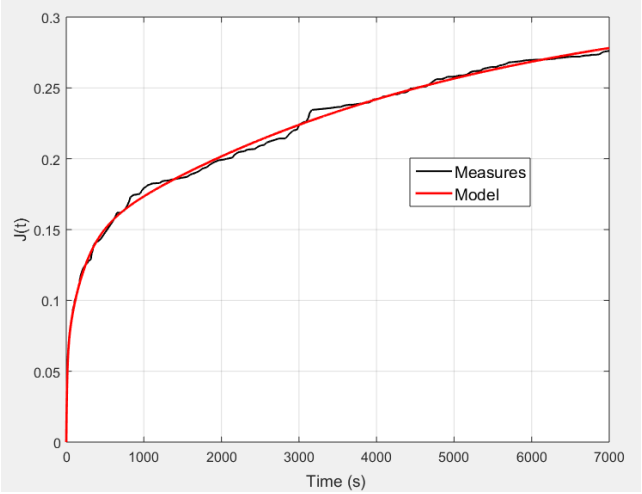

Figure 9. Fitting experimental deformation data of a tight sandstone sample under axial stress of 10 Mpa: Measures presented in [41, Figure 3.b] (black), $F(s)$ fitting (red) with $N = 4$.

However, as described in the introduction, fractional models may present several challenges These challenges including: lack of clear physical interpretation of fractional parameters, structural non-uniqueness, numerical difficulties, multiplicity of definitions of fractional derivatives, physical inconsistency of initial conditions and the risk of misinterpreting fractional behaviors. It is thus of interest to develop alternative methods that enable equally accurate modelling with an equivalent number of parameters, but without introducing the complex concepts related to fractional calculus. The objective of the following section paragraph is to address this.

3.3. Fractional dynamical behavior modelling using DRT

Instead of directly reconstructing the DRT kernel $G(\tau)$ (for any value of τ) with the algorithm of Section 3.1, we propose, in this section to impose a structure on this kernel and to search for the parameters that define this structure.

In the following, it is assumed that the models used are based on distributions of the logarithm of the time constant and defined by:

$$H(j\omega) = \int_0^\infty \frac{G(\tau)}{1+j\omega\tau}\, d\tau = \int_0^\infty \frac{g(\tau)}{1+j\omega\tau}\, dln(\tau) \quad \text{with} \quad G(\tau) = \frac{g(\tau)}{\tau}, \tag{42}$$

where the kernel $g(\tau)$ follows a symmetric log-normal distribution with three independent parameters ($a \in \mathbb{R}_+^*,\ m \in \mathbb{R},\ \sigma \in \mathbb{R}_+^*$) of the form

$$g(\tau) = ae^{\left(-\frac{(ln(\tau)-m)^2}{2\sigma^2}\right)}. \tag{43}$$

alternatively, an asymmetric log-normal distribution with four independent parameters ($a \in \mathbb{R}_+^*$, $m \in \mathbb{R},\ \sigma \in \mathbb{R}_+^*,\ \lambda \in \mathbb{R}$)

$$g(\tau) = ae^{\left(-\frac{(ln(\tau)-m)^2}{2\sigma^2}\right)}\left(1 + erf\left(\lambda\frac{ln(\tau)-m}{\sqrt{2\sigma}}\right)\right) \tag{44}$$

or modulated log-normal distributions with five independent parameters ($\in \mathbb{R}_+^*,\ m \in \mathbb{R},\ \sigma \in \mathbb{R}_+^*$, $\lambda \in \mathbb{R},\ \phi \in \mathbb{R}$)

$$g(\tau) = ae^{\left(-\frac{(ln(\tau)-m)^2}{2\sigma^2}\right)}cos(\omega(ln(\tau)-m)+\phi). \tag{45}$$

In these expressions, the log-normal distribution can be replaced by alternative distributions presented in the Appendix A.1.

The system considered in this section is based on Love wave gas sensors developed in [43,44]. These sensors rely on the propagation of a guided shear horizontal surface acoustic wave (SH-SAW), known as a Love wave, which is confined within a guiding layer deposited on a piezoelectric substrate. The operating principle is as follows. A sinusoidal electrical signal $V_e(t)$ is applied to an Interdigital Transducer (IDT), generating an acoustic wave through the inverse piezoelectric effect. This wave propagates along the surface of the device, with particle displacement parallel to the surface and perpendicular to the propagation direction. A sensitive layer is deposited on the propagation path between the transmitting and receiving IDTs. When target gas molecules are adsorbed onto this layer, they induce changes in its mass density and viscoelastic properties. These modifications affect the velocity and attenuation of the acoustic wave. The resulting perturbation is detected at the receiving IDT, where the acoustic wave is converted back into an electrical signal $V_s(t)$. The presence of the target gas induces measurable variations in the phase and/or frequency of the signal, which can be correlated to the gas concentration. Due to the confinement of the acoustic energy near the surface, Love wave devices exhibit enhanced sensitivity to surface perturbations, making them particularly suitable for gas sensing applications.

The experimental measurements used in this study are obtained from Love wave sensors coated with graphene oxide (GO) films deposited by inkjet printing, as reported in [44]. Gas detection experiments are performed using a controlled vapor generation system, where a constant nitrogen flow (0.112 L/min) is used as a carrier gas to deliver toluene vapors into a sealed chamber containing the sensor. The

concentration of toluene varies in a controlled manner, and the sensor response is monitored through the frequency shift of the acoustic wave. The adsorption of toluene molecules onto the sensitive layer induces a measurable frequency variation, with a reported sensitivity of approximately 24 Hz/ppm. The steady-state response shows a linear dependence on gas concentration, while the transient response reflects adsorption and desorption kinetics.

These dynamic responses, particularly for step variations in concentration, are used in this work to analyze the long-memory behavior of the sensor and to validate the proposed DRT-based modelling approach.

The experimental measurements carried out are plotted in Figure 10 for the toluene sensor. They represent the frequency deviation measured in response to a 1 ppm increase in toluene at $t = 0s$.

The experimental data in Figure 10 show input-output behavior similar to that of Figure 7, suggesting a potentially fractional behavior. The model defined by relation (42) in which the function $g(\tau)$ is defined by relation (42) is used to fit the time response of Figure 10 considered as the response to a step input. The system output is thus defined by

$$\tilde{V}_s(t) = \int_0^\infty g(\tau)\left(1 - e^{-\frac{t}{\tau}}\right) dln(\tau). \tag{46}$$

For a numeric implementation, the change of variable $\tau = e^x$ and thus $dln(\tau) = dx$ is first used leading for relation (46) to

$$\tilde{V}_s(t) = \int_{-\infty}^\infty g(e^x)\left(1 - e^{-\frac{t}{e^x}}\right) dx. \tag{47}$$

Relation (47) can be discretized using Euler's formula (but more complex numerical schemes can be used) on the interval $x \in [x_{min}, x_{max}]$. This interval can also be defined by $x \in [M - L\sigma, M + L\sigma]$ in the case where kernel $g(\tau)$ is defined by relation (43) to capture > 99.999% of the Gaussian function. Relation (47) is thus approximated by

$$\tilde{V}_s(t) \approx \sum_{i=0}^{N_x} g(e^{x_i})\left(1 - e^{-\frac{t}{e^{x_i}}}\right)\Delta x \tag{48}$$

with

$$x_i = x_{min} + i\Delta x, \qquad \Delta x = \frac{x_{min} - x_{max}}{N_x + 1}. \tag{49}$$

Parameters a, m, σ in relation (42) are computed by solving a nonlinear optimization problem (Levenberg–Marquardt algorithm) aimed at minimizing the error

$$\varepsilon = \sum_{k=1}^{N_t+1} \frac{\left(V_s(t_k) - \tilde{V}_s(t_k)\right)^2}{N_t}, \qquad t_k = k\Delta t, \qquad \Delta t = \frac{x_{min} - x_{max}}{N_t + 1}. \tag{50}$$

The optimal parameters obtained are:

$$a = 585.27, \qquad m = 4.5, \qquad \sigma = 8.78. \tag{51}$$

Figure 10 shows a comparison of the sensor response with the response of model (42) with relation (43) for $g(\tau)$ and highlights that this model captures accurately the sensor behavior. Moreover, the representation of kernel $g(\tau)$ in Figure 10 fully justifies the fact that the sensor's behavior cannot be modeled with one or a few exponential functions.

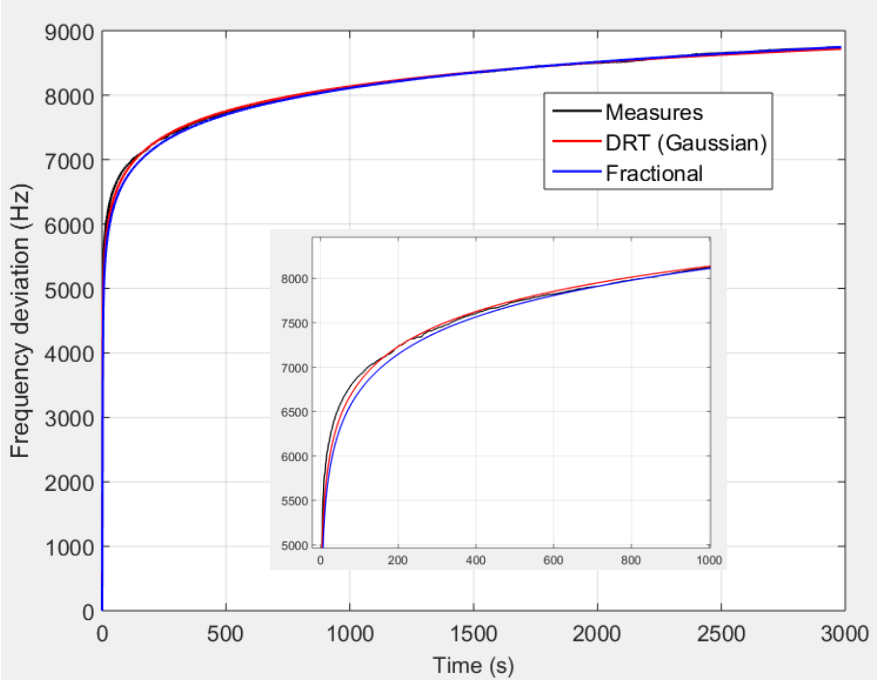

Figure 10. Sensor response $V_s(t)$ to an increase in toluene levels (black) compared to the DRT based model with log-normal kernel response (red) and to the fractional model response (blue).

This modelling approach is compared to modelling using a fractional model of the transfer function

$$F(p) = \frac{K_f}{\frac{s^\alpha}{\omega_f} + 1} \tag{52}$$

thus with three parameters $K_f \in \mathbb{R}_+^*$, $\omega_f \in \mathbb{R}_+^*$, $\alpha \in [0,1]$ as for model (42) with (43) for $g(\tau)$. They are also computed by solving a nonlinear optimization problem (Levenberg–Marquardt algorithm) minimizing the error (50). The optimal parameters obtained are:

$$K_f = 482.78, \qquad \omega_f = 0.373, \qquad \alpha = 0.164. \tag{53}$$

This model response to a step variation of toluene concentration is represented by Figure 11 and compared with the response of the sensor and of the DRT-based model (42). These comparisons reveal that the accuracy of the two models is similar, with a slight improvement for the DRT-based model (41). This is confirmed by the value of the error (50) obtained with the two optimal models:

- DRT-based model: $\varepsilon = 1.321 \times 10^8$;
- Fractional model: $\varepsilon = 1.662 \times 10^8$.

However, compared to the fractional model, the DRT based model has two major advantages.

1. It is not necessary to use fractional calculus, which is a complex concept and, as indicated in the introduction, is now associated with several limitations, especially when initial conditions need to be taken into account.
2. The DRT-based model enables a consistent physical interpretation [45]. The gaussian kernel $g(\tau)$ clearly defines the distribution of time constants with which toluene molecules bind to the sensitive layer.

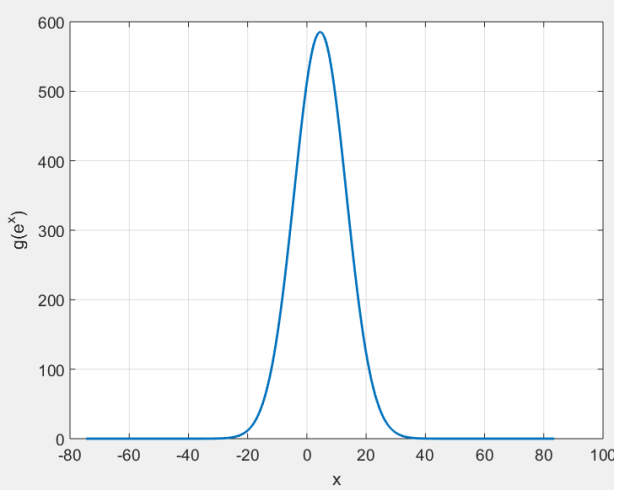

Figure 11. Representation of kernel $g(\tau)$ with parameters given by relation (51).

Beyond this application, more general interpretations are permitted to explain why a DRT with a log-normal law allows for a proper fit of fractional behaviors. In the field of statistics, a log-normal process [45,46] is the statistical realisation of the multiplicative product of many independent random variables, each of which is positive. Let y be the product of n independent and identically distributed random variables such that:

$$y = x_1 x_2 \dots x_n, \tag{54}$$

the logarithm of y is given by:

$$z = log(y) = \sum_{k=1}^{n} log(x_k). \tag{55}$$

According to the central limit theorem, for large n, z approximates a normal distribution:

$$z = log(y) \sim \mathcal{N}(m, \sigma^2) \tag{56}$$

in which m and σ^2 denote respectively the mean and variance of $log(y)$.

This property explains why fractional behaviors can be captured by a DRT with a log-normal distribution. It also explains why fractional models that combine Cole-Cole terms can also be used for this type of behaviors, since, as illustrated in Figure A.2, a Cole-Cole model reduces to a DRT with a distribution similar to a log-normal law.

Indeed, in the case of diffusion, the diffusion time constant meets locally $\tau = L^2/D$ where L is the path length and D is the diffusion coefficient. In a disordered medium:

$$L = L_0 \times tortuosity \times porosity \times geometric\ factor \tag{57}$$

and thus the time constants τ in the disordered medium are a product of several random factors. They thus follow a log-normal distribution.

Also, for an electrode, the time constant is defined locally by $\tau = R_{ct} C_{dl}$ where R_{ct} denotes the charge transfer resistance and C_{dl} is the double layer capacitance with

$$R_{ct} \propto \frac{1}{i_0 A} \qquad \text{and} \qquad C_{dl} \propto A, \tag{58}$$

where A is the local surface and i_0 is the local exchange current density. But in a real porous medium, i_0 varies locally and

$$i_0 = f(surface, tortuosity, diffusion, kinetics, \ldots). \tag{59}$$

Thus in the porous electrode,

$$\tau \propto (size\ \ of\ \ pores)^{\alpha}(tortuosity)^{\beta}(porosity)^{\gamma}. \tag{60}$$

The time constants τ in the porous medium are thus a product of several random factors. They thus follow a log-normal distribution

4. Paper contributions, novelty and new mathematical insights

Having reached the end of this study, it is possible to take stock of the contributions and new features introduced.

- **Link DRT/diffusive representation.** At the best of our knowledge, no paper establishes explicitly this link and the relationships to transition from one to the other. The paper provides the exact mathematical connection to pass directly between the DRT framework and Montseny's diffusive representation.
- **DRT as a model discriminator.** We propose using the structure of the DRT itself, prior to any identification, to discriminate between fractional-order and other model (in particular fractional) model classes. To the best of our knowledge, this specific diagnostic application of the DRT for a priori model selection is absent from the published literature.
- **Physically inspired analytical DRT as an alternative solution for fractional behavior.** There is no article in the literature that presents DRT as a viable alternative to fractional models for capturing the input-output behavior of fractional behaviors. This possible alternative is highlighted in this paper.
- **Analytical DRT identification for sensors.** We acknowledge the recent work on reconstructing DRTs with analytical basis functions [47]. However, the nature of the functions used is completely different and allows for physical interpretations. Furthermore, [47] is dedicated to the frequency domain, while the proposed method and algorithms are applied in the time domain and demonstrate their effectiveness in capturing the input-output behavior of systems exhibiting fractional behavior.
- **Direct time-domain scheme.** We formulate a direct time-domain algorithm that extracts continuous relaxation distributions from raw input-output data without requiring frequency-domain conversion.
- **Time-domain Volterra inversion.** We show that the DRT deconvolution problem can be formulated and solved entirely in the time-domain as a Volterra integral equation of the first kind, bypassing the need for noisy numerical Fourier/Laplace conversions.
- **Statistical genesis of power-laws.** By leveraging the multiplicative Central Limit Theorem, it is demonstrated mathematically how a log-normal distribution of standard integer-order Debye relaxations asymptotically generates apparent fractional power-law behaviors, providing a rigorous statistical physics alternative to abstract fractional-order postulates.

5. Conclusions

In this paper, we have analyzed the interest of DRT modelling in the context of fractional dynamic

or kinetic behaviors. We first examined the relationships between diffusive representations and infinite-state formulations, demonstrating that these approaches provide different but equivalent expressions of a common spectral decomposition framework for linear systems with memory. By representing system dynamics as a continuous or discrete superposition of elementary exponential modes, these formulations offer a highly interpretable, physically consistent, and mathematically tractable way to analyze complex dynamical behaviors such as fractional behaviors.

The various case studies presented in this work, ranging from viscoelasticity to gas sensors and epidemiological data, demonstrate that DRT analysis serves as a powerful diagnostic tool for understanding the true origin of behaviors that are too often automatically interpreted as fractional. In many instances, the analysis reveals that observed power-law or long-memory dynamics can be accurately reproduced by a narrow, finite distribution of relaxation times. This indicates that relatively simple integer-order models, expressed as sums of exponential responses, are frequently sufficient to describe the system behavior with high accuracy, without the need for complex fractional operators. DRT therefore appears as a crucial diagnostic tool against model misuse.

These results strongly suggest that the use of fractional-order models should no longer be considered a default modelling strategy simply because power-law-like responses are observed. Apparent fractional behaviors may merely emerge from the superposition of a limited number of exponential mechanisms over a restricted time or frequency range. In such situations, fractional models do not provide additional physical insight; worse, they can lead to misleading interpretations of the underlying physical mechanisms and introduce unnecessary numerical and structural complexities (such as initial condition inconsistencies).

Consequently, we advocate a methodological shift: DRT-based analysis should become a systematic preliminary step before adopting any fractional modelling approach. This enables researchers to identify the true structure of the relaxation spectrum and determines whether a fractional formulation is genuinely justified, or if an equivalent, more interpretable integer-order representation should be preferred.

Moreover, as demonstrated through the gas sensor application, combining the DRT framework with specific continuous structures (such as log-normal distributions) provides a powerful and direct alternative to fractional models. The proposed numerical scheme offers a major advantage over traditional deconvolution methods by operating entirely in the time domain using raw input-output data, thereby avoiding the numerical noise and artifacts induced by Fourier or Laplace transforms. Quantitatively, for the Love wave gas sensor case study, the log-normal DRT model achieves an excellent fit with an optimization error of $\varepsilon = 1.321 \times 10^8$, which is slightly lower than that of the fractional-order model ($\varepsilon = 1.662 \times 10^8$) while using the exact same number of parameters (three parameters).

This approach matches the predictive accuracy of fractional transfer functions while avoiding the mathematical complexities, structural non-uniqueness, and initial condition inconsistencies associated with fractional calculus. Crucially, unlike the often-abstract parameters of fractional models, the parameters of a log-normal DRT offer clear, consistent physical interpretations. They directly reflect the statistical distribution of underlying microscopic processes, such as the varied time constants of molecular binding or diffusion in disordered media, which naturally emerge from the multiplicative product of numerous random physical factors. The proposed numerical scheme thus offers several advantages over existing methods:

- It operates directly on time-domain data and does not require frequency-domain measurements.
- Tikhonov regularization ensures a smooth, physically interpretable DRT even with noisy data.
- It accommodates different kernel structures depending on the physical context.
- It is a serious alternative to fractional systems, offering equivalent precision.

To further establish DRT and diffusive representations as robust and transparent alternatives, future work should focus on:

- The development of automated identification tools: Providing the community with standardized algorithms to extract DRT directly from noisy time-domain and frequency-domain data, making the diagnostic step accessible to non-specialists.
- Extension to non-linear and time-varying systems: Investigating how the DRT framework can be adapted to capture phenomena where relaxation times drift due to aging, temperature, or varying operating conditions.
- Physical correlation: Further deepening the links between the extracted structural parameters of the DRT (such as the parameters of the log-normal kernels) and the microscopic physical or chemical properties of the studied materials.
- Exploration of generalized DRT frameworks: Replacing the elementary Debye relaxation kernel by fractional kernels like the Cole-Cole or Davidson-Cole models to open new paths for combining distributed parameter models with non-ideal relaxation mechanisms.

Author contributions

Jocelyn SABATIER: Conceptualization, methodology, validation, formal analysis, writing–original draft preparation, writing–review and editing, Writing-review and editing of Section 3.3; Hamida HALLIL: Data input of Section 3.3, writing–review and editing of Section 3.3. All authors have read and approved the final version of the manuscript for publication.

Use of Generative-AI tools declaration

The authors declare they have not used Artificial Intelligence (AI) tools in the creation of this article.

Conflict of interest

The authors declare no conflicts of interest.

References

1. M. Wiśniewski, J. Łuczka, J. Spiechowicz, Memory corrections to Markovian Langevin dynamics, *Entropy*, **26** (2024), 425. https://doi.org/10.3390/e26050425
2. S. Brandani, S. Hwang, J. Kärger, E. Mangano, Diffusion anomaly in nanopores as a rich field for theorists and a challenge for experimentalists, *Nature Commun.*, **15** (2024), 5721. https://doi.org/10.1038/s41467-024-49821-w
3. A. Klimek, B. A. Dalton, R. R. Netz, Subdiffusion from competition between multi-exponential friction memory and energy barriers, *Eu.r Phys. J. E*, **48** (2025). https://doi.org/10.1140/epje/s10189-025-00518-y
4. I. Podlubny, Geometric and physical Interpretation of fractional Integration and fractional differentiation, *Fract. Calc. Appl. Anal.*, **5** (2002), 367–386. https://doi.org/10.48550/arXiv.math/0110241
5. V. Tarasov, Geometric interpretation of fractional-order derivative, *Fract. Calc. Appl. Anal.*, **19** (2016), 1200–1221. https://doi.org/10.1515/fca-2016-0062

6. J. Sabatier, C. Farges, V. Tartaglione, *Fractional behaviours modeling: Analysis and application of several unusual tools*, Intelligent Systems, Control and Automation: Science and Engineering series, Cham, Switzerland: Springer, **101** (2022). https://doi.org/10.1007/978-3-030-96749-9
7. A. M. Balint, S. Balint, Mathematical description of the groundwater flow and that of the impurity spread, which use temporal Caputo or Riemann-Liouville fractional partial derivatives, is non-objective, *Frac. Fract.*, **4** (2020), 36. https://doi.org/10.3390/fractalfract4030036
8. A. Dokoumetzidis, R. Magin, P. A. Macheras, Commentary on fractionalization of multi-compartmental models, *J. Pharmaconet. Phar.*, **37** (2010), 203–207. https://doi.org/10.1007/s10928-010-9153-5
9. Pantokratoras, Comment on the paper "Fractional order model of thermo-solutal and magnetic nanoparticles transport for drug delivery applications, Subrata Maiti, Sachin Shaw, G.C. Shit, *Colloid. Surface. B*, **222** (2023), 113074. https://doi.org/10.1016/j.colsurfb.2022.113074
10. M. Caputo, M. Fabrizio, A new definition of fractional derivative without singular kernel, *Prog. Fract. Different. Appl.*, **1** (2015), 73–85. https://doi.org/10.12785/pfda/010201
11. A. Atangana, D. Baleanu, New fractional derivatives with nonlocal and non-singular kernel: Theory and application to heat transfer model, *Therm. Sci.*, **20** (2016), 763–769. https://doi.org/10.2298/TSCI160111018A
12. J. Hristov, *Derivatives with non-singular Kernels from the Caputo-Fabrizio definition and beyond: Appraising analysis with emphasis on diffusion models*, In: Frontiers in Fractional Calculus, Chapter 10, edited by Sachin Bhalekar, Bentham Science Publishers, 2017. https://doi.org/10.2174/9781681085999118010013
13. J. Sabatier, M. Merveillaut, R. Malti, A. Oustaloup, How to impose physically coherent initial conditions to a fractional system? *Commun. Nonlinear Sci. Numer. Simul.*, **15** (2010), 1318–1326. https://doi.org/10.1016/j.cnsns.2009.05.070
14. M. D. Ortigueira, F. Coito, System initial conditions vs derivative initial conditions, *Comput. Math. Appl.*, **59** (2010), 1782–1789. https://doi.org/10.1016/j.camwa.2009.08.036
15. J. Sabatier, Fractional order models are doubly infinite dimensional models and thus of infinite memory: Consequences on initialization and some solutions, *Symmetry*, **13** (2021), 1099. https://doi.org/10.3390/sym13061099
16. A. V. Milovanov, K. Rypdal, J. J. Rasmussen, Stretched exponential relaxation and ac universality in disordered dielectrics, *Phys Rev B*, **76** (2007), 104201. https://doi.org/10.1103/PhysRevB.76.104201
17. E. C. de Oliveira, J. A. T. Machado, A review of definitions for fractional derivatives and integral, *Math. Probl. Eng.*, **2014** (2014), 238459. https://doi.org/10.1155/2014/238459
18. C. Plank, T. Rüther, L. Jahn, M. Schamel, J. P. Schmidt, F. Ciucci, et al., A review on the distribution of relaxation times analysis: A powerful tool for process identification of electrochemical systems, *J. Power Sources*, **594** (2024), 233845. https://doi.org/10.1016/j.jpowsour.2023.233845
19. G. Montseny, Diffusive representation of pseudo-differential time-operators, *ESAIM Pro. Surveys*, **5** (1998), 159–175. https://doi.org/10.1051/proc:1998005
20. G. Montseny, *Representation diffusive*, Hermès Science, 2005.
21. M. Saccoccio, T. H. Wan, C. Chen, F. Ciucci, Optimal regularization in distribution of relaxation times applied to electrochemical impedance spectroscopy: Ridge and Lasso regression methods–A theoretical and experimental study, *Electrochimica Acta*, **147** (2014), 470–482. https://doi.org/10.1016/j.electacta.2014.09.058

22. T. H. Wan, M. Saccoccio, C. Chen, F. Ciucci, Influence of the discretization as well as the linear and nonlinear regularization on the distribution of relaxation times, *Electrochimica Acta*, **184** (2015), 483–499. https://doi.org/10.1016/J.ELECTACTA.2015.09.097
23. E. H. Balaguera, A full capacitive picture of the constant phase element: Estimations from impedance spectroscopy, distribution of relaxation times and fractional calculus, *Electrochem. Commun.*, **180** (2025), 108053, https://doi.org/10.1016/j.elecom.2025.108053
24. A. Allagui, A. S. Elwakil, Procedure for obtaining the analytical distribution function of relaxation times for the analysis of impedance spectra using the fox H-function, *J. Phys. Chem. C*, **128** (2024), 2788–2795. https://doi.org/10.1021/acs.jpcc.3c08411
25. M. D. Ortigueira, V. Martynyuk, V. Kosenkov, A. G. Batista, A new look at the capacitor theory, *Fractal Fract.*, **7** (2023), 86. https://doi.org/10.3390/fractalfract7010086
26. M. D. Ortigueira, *Fractional calculus for fractional signals and systems*, Springer Science and Business Media, 2011. https://doi.org/10.1007/978-94-007-0747-4
27. W. A. Yager, The distribution of relaxation times in typical dielectrics, *J. Appl. Phys.*, **7** (1936), 434–450. https://doi.org/10.1063/1.1745355
28. K. S. Cole, R. H. Cole, Dispersion and absorption in dielectrics I. Alternating current characteristics, *J. Chem. Phys.*, **9** (1941), 341–351. https://doi.org/10.1063/1.1750906
29. R. M. Fuoss, J. G. Kirkwood, Electrical properties of solids VIII. Dipole moments in polyvinyl Chloride-Diphenyl systems, *J. Am. Chem. Soc.*, **63** (1941), 385–394. https://doi.org/10.1021/ja01847a013
30. P. Debye, *Polar molecules*, New York: The Chemical Catalogue Company, 1929. https://doi.org/10.1002/jctb.5000484320
31. K. T. Malkow, Analytical inversion of complex-valued DRT in impedance spectroscopy by integral transforms, *Electrochimica Acta*, **535** (2025), 146500. https://doi.org/10.1016/j.electacta.2025.146500
32. J. R. Macdonald, Impedance spectroscopy: Old problems and new developments, *Electrochimica Acta*, **35** (1990), 1483–1492. https://doi.org/10.1016/0013-4686(90)80002-6
33. E. Tuncer, J. R. Macdonald, Comparison of methods for estimating continuous distributions of relaxation times, *J. Appl. Phys.*, **99** (2006), 074106. https://doi.org/10.1063/1.2188053
34. T. H. Wan, M. Saccoccio, C. Chen, F. Ciucci, Influence of the discretization methods on the distribution of relaxation times deconvolution: Implementing radial basis functions with Tikhonov regularization, *Electrochimica Acta*, **184** (2015), 483–499. https://doi.org/10.1016/j.electacta.2015.09.097
35. R. Ebead, B. Abo-Zalam, E. Nabil, System identification of photovoltaic system based on fractional-order model, *J. Comput. Electron.*, **22** (2023), 471–484. https://doi.org/10.1007/s10825-022-01996-5
36. Y. Chen, F. Liu, Q. Yu, T. Li, Review of fractional epidemic models, *Appl. Math. Model.*, **97** (2021), 281–307. https://doi.org/10.1016/j.apm.2021.03.044
37. P. A. Naik, M. Farman, K. Jamil, K. S. Nisar, M. A. Hashmi, Z. Huang, Modeling and analysis using piecewise hybrid fractional operator in time scale measure for ebola virus epidemics under Mittag–Leffler kernel, *Sci. Rep.*, **14** (2024), 24963. https://doi.org/10.1038/s41598-024-75644-2
38. A. Oustaloup, F. Levron, S. Victor, L. Dugard, Non-integer (or fractional) power model to represent the complexity of a viral spreading: Application to the COVID-19, *Annu. Rev. Control*, **52** (2021), 523–542. https://doi.org/10.1016/j.arcontrol.2021.09.003

39. A. Oustaloup, F. Levron, S. Victor, L. Dugard, From the FPM model in viral spreading to predictions of CO_2 concentration in the atmosphere, *Nonlinear Dynam.*, **114** (2026), 17. https://doi.org/10.1007/s11071-025-12033-y
40. A. Oustaloup, F. Levron, S. Victor, L. Dugard, Addendum: Predictive form of the FPM model, *Annu. Rev. Control*, **55** (2023), 291–296. https://doi.org/10.1016/j.arcontrol.2023.02.001
41. X. Ding, G. Zhang, B. Zhao, Y. Wang, Unexpected viscoelastic deformation of tight sandstone: Insights and predictions from the fractional Maxwell model, *Sci. Rep.*, **7** (2017), 11336. https://doi.org/10.1038/s41598-017-11618-x
42. A. Allagui, A. Elwakil, Generalized distribution function of relaxation times with the Davidson-Cole model as a Kernel, *Adv. Theor. Simul.*, **8** (2025), e00792. https://doi.org/10.1002/adts.202500792
43. I. Nikolaou, H. Hallil, V. Conédéra, B. Plano, O. Tamarin, J. L. Lachaud, et al., Electro-mechanical properties of inkjet-printed graphene oxide nanosheets, *Phys. Status Solidi A*, **214** (2017), 1600492. https://doi.org/10.1002/pssa.201600492
44. I. Nikolaou, H. Hallil, V. Conédéra, G. Deligeorgis, C. Dejous, D. Rebiere, Inkjet-printed graphene oxide thin layers on love wave devices for humidity and vapor detection, *IEEE Sens. J.*, **16** (2016), 7620–7627. https://doi.org/10.1109/JSEN.2016.2600269
45. J. Sabatier, Probabilistic interpretations of fractional operators and fractional behaviours: Extensions, applications and tribute to Prof. José Tenreiro Machado's ideas, *Mathematics*, **10** (2022), 4184. https://doi.org/10.3390/math10224184
46. E. Limpert, W. A. Stahel, M. Abbt, Log-normal Distributions across the sciences: Keys and clues: On the charms of statistics, and how mechanical models resembling gambling machines offer a link to a handy way to characterize log-normal distributions, which can provide deeper insight into variability and probability—normal or log-normal: That is the question, *BioScience*, **51** (2001), 341–352. https://doi.org/10.1641/0006-3568(2001)051[0341:LNDATS]2.0.CO;2
47. R. Leonhardt, J. K. von Nidda, D. Andrae, A. Schmidt, J. Kowal, T. Tichter, Reconstructing the distribution of relaxation times with analytical basis functions, *J. Power Sources*, **652** (2025), 237403. https://doi.org/10.1016/j.jpowsour.2025.237403
48. J. Sabatier, C. Farges, J. C. Trigeassou, Fractional systems state space description: Some wrong ideas and proposed solutions, *J. Vib. Control*, **20** (2014), 1076–1084. https://doi.org/10.1177/1077546313481839
49. D. Zwillinger, V. Moll, *Table of integrals, series, and products*, Academic Press, 2014, https://doi.org/10.1016/c2013-0-10754-4
50. A. Erdelyi, *Tables of integral transforms*, McGraw-Hill, **1** (1954).
51. M. Abramowitz, I. Stegun, *Handbook of mathematical functions, graphs, and mathematical tables*, National Bureau of Standards, 1964.

Appendix

A.1. Some kernels for DRT based modelling

In this section, we propose several alternative kernels $g(\tau)$ to those given in Section 3.4 for a DRT-based model whose frequency response is defined by:

$$H(j\omega) = \int_0^\infty \frac{g(\tau)}{1+j\omega\tau}\, dln(\tau). \tag{A.1}$$

Lorentzian function. Three parameters with a broader peak than a Gaussian function and a long tail:

$$g(\tau) = \frac{a}{1 + \left(\frac{ln(\tau) - m}{\sigma}\right)^2}. \tag{A.2}$$

Generalised-gaussian function. $\beta < 2$ sharper peaks, $\beta > 2$ more flattened, $\beta = 1$ exponential decay

$$g(\tau) = ae^{\left(-\frac{|ln(\tau)-m|^\beta}{2\sigma^2}\right)}. \tag{A.3}$$

sech ²function. Narrower profile than the Gaussian:

$$g(\tau) = asech^2\left(\frac{ln(\tau) - m}{\sigma}\right). \tag{A.4}$$

These various kernels are represented in Figure A.1 for $m = 1$.

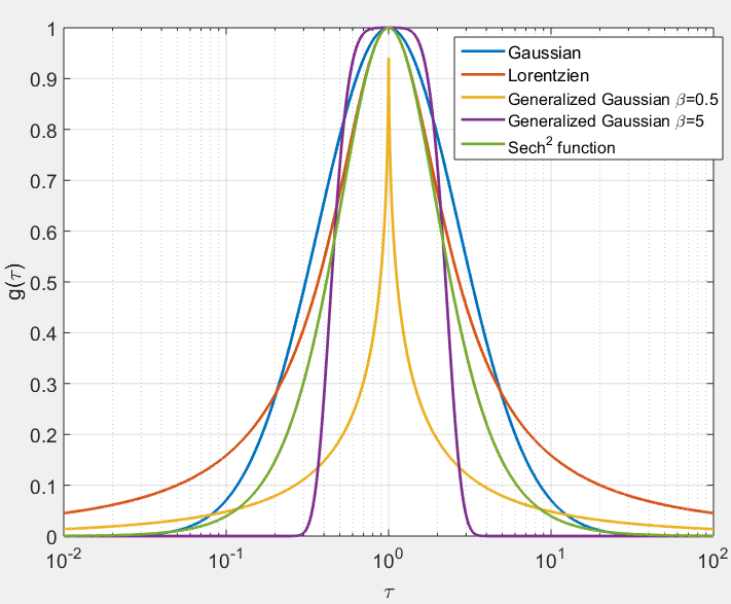

Figure A.1. Representation of kernels $g(\tau)$ proposed in Section A.1.

A.2. DRT representation of some integer and fractional models

Due to the link between diffusive representation and DRT-based representation described in Section 2.2 and recalled here:

$$\mu(\xi) = \frac{1}{\xi} G\left(\frac{1}{\xi}\right) \text{ and thus } G(\tau) = \frac{1}{\tau}\mu\left(\frac{1}{\tau}\right), \tag{A.5}$$

the relation being obtained using the change of variable $\xi = 1/\tau$, this section provides the frequency representation of several fractional transfer functions under the DRT form

$$H(j\omega) = \int_0^\infty \frac{G(\tau)}{1+j\omega\tau}\, d\tau = \int_0^\infty \frac{g(\tau)}{1+j\omega\tau}\, dln(\tau) \text{ thus } G(\tau) = \frac{g(\tau)}{\tau}. \tag{A.6}$$

The information presented in this section is based on results presented in tables in [19,36] in the

context of diffusive representation. All generalized impedance and admittance transfer functions listed below are evaluated along the imaginary axis via the substitution $s \to j\omega$. For bounded fractional systems, the derivation of the diffusive representations and DRT kernels can be established using contour integration methods as detailed in [48]. For the pure fractional integrator ($a = 0$ in [48]), it can be derived directly via complex integration (using Cauchy's residue theorem along a Bromwich contour with a branch cut along the negative real axis) or through the known Laplace/Stieltjes integral identity $\int_0^\infty (\tau^{\nu-1}/(1+s\tau))\, d\tau = \pi s^{-\nu}/sin(\nu\pi)$, $s > 0$ and $0 < \nu < 1$. In this appendix, to rigorously confirm the validity of all expressions, the integral relation:

$$H(s) = \int_0^\infty \frac{G(\tau)}{1+s\tau}\, d\tau \tag{A.7}$$

is evaluated for each kernel $G(\tau)$ while verifying that the correct function $H(s)$ is obtained. The resulting impulse response of the considered fractional transfer functions is also provided.

A.2.1. Integer model with two poles (for proof see relations (9) to (11))

Transfer function: $H(s) = \frac{A}{\tau_1 s+1} + \frac{B}{\tau_2 s+1}$.

DRT-based frequency response: $H(j\omega) = \int_0^\infty \frac{G(\tau)}{1+j\omega\tau}\, d\tau$.

DRT kernel: $G(\tau) = A \cdot \delta(\tau - \tau_1) + B \cdot \delta(\tau - \tau_2)$.

Order ν fractional integrator or Constant Phase Element (CPE)

Transfer function: $H(s) = \frac{1}{\left(\frac{s}{\omega_0}\right)^\nu}$, $0 < \nu < 1$, $\omega_0 \in \mathbb{R}_+^*$.

DRT-based frequency response: $H(j\omega) = \int_0^\infty \frac{G(\tau)}{1+j\omega\tau}\, d\tau$.

DRT kernel: $G(\tau) = (\omega_0)^\nu \frac{\sin(\nu\pi)}{\pi} \tau^{\nu-1}$.

Proof.

$$\int_0^\infty \frac{G(\tau)}{1+s\tau}\, d\tau = (\omega_0)^\nu \frac{\sin(\nu\pi)}{\pi} \int_0^\infty \frac{\tau^{\nu-1}}{1+s\tau}\, d\tau. \tag{A.8}$$

Using the standard integral [49, §3.241.2]

$$\int_0^\infty \frac{x^{\alpha-1}}{1+\beta x}\, dx = \frac{\pi}{\beta^\alpha \sin(\alpha\pi)}, \qquad 0 < \alpha < 1, \tag{A.9}$$

with $\alpha = \nu$ and $\beta = s$, then

$$\int_0^\infty \frac{\tau^{\nu-1}}{1+s\tau}\, d\tau = \frac{\pi\, s^{-\nu}}{\sin(\nu\pi)}. \tag{A.10}$$

Hence

$$\int_0^\infty \frac{G(\tau)}{1+s\tau}\, d\tau = (\omega_0)^\nu \frac{\sin(\nu\pi)}{\pi} \cdot \frac{\pi\, s^{-\nu}}{\sin(\nu\pi)} = (\omega_0)^\nu s^{-\nu} = \frac{1}{\left(\frac{s}{\omega_0}\right)^\nu} = H(s). \tag{A.11}$$

■

A.2.2. Davidson-Cole or fractional Debye

Transfer function: $H(s) = \frac{1}{\left(\frac{s}{\omega_l}+1\right)^{\nu}},\ 0 < \nu < 1,\ \omega_l \in \mathbb{R}_+^*$.

DRT-based frequency response: $H(j\omega) = \int_0^{\infty} \frac{G(\tau)}{1+j\omega\tau}\, d\tau$.

DRT kernel: $G(\tau) = \frac{\sin(\nu\pi)}{\pi} \frac{\tau^{\nu-1}{\omega_l}^{\nu}}{(1-\omega_l\tau)^{\nu}}$ if $\tau \le \frac{1}{\omega_l}$ else $G(\tau) = 0$.

Proof.

First, use the change of variable $u = \omega_l\tau$. Then $\tau = u/\omega_l$, $d\tau = du/\omega_l$, and the limits become $u = 0$ to $u = 1$. With $s \to j\omega$, the integral (A.7) becomes

$$H(s) = \frac{\sin(\nu\pi)}{\pi} \int_0^1 \frac{u^{\nu-1}}{(1-u)^{\nu}} \frac{1}{1+(s/\omega_l)u}\, du. \tag{A.12}$$

Now, use

$$u = \frac{x}{1+x}, \tag{A.13}$$

then

$$1-u = \frac{1}{1+x}, \qquad du = \frac{1}{(1+x)^2}\, dx, \tag{A.14}$$

and the limits become $x = 0$ to $x = \infty$. Computing the various factors, leads to:

$$u^{\nu-1} = \left(\frac{x}{1+x}\right)^{\nu-1} = x^{\nu-1}(1+x)^{-(\nu-1)}, \tag{A.15}$$

$$(1-u)^{-\nu} = (1+x)^{\nu}, \tag{A.16}$$

$$\frac{1}{1+(s/\omega_l)u} = \frac{1}{1+(s/\omega_l)\frac{x}{1+x}} = \frac{1+x}{1+x+(s/\omega_l)x} = \frac{1+x}{1+(1+s/\omega_l)x}. \tag{A.17}$$

Multiplying these factors together with du leads to:

$$\begin{aligned} u^{\nu-1}(1-u)^{-\nu} \frac{1}{1+(s/\omega_l)u}\, du \\ = x^{\nu-1}(1+x)^{-(\nu-1)}(1+x)^{\nu} \frac{1+x}{1+(1+s/\omega_l)x} \frac{1}{(1+x)^2}\, dx. \end{aligned} \tag{A.18}$$

Simplify the powers of $(1+x)$ gives

$$-(\nu-1)+\nu+1-2 = -\nu+1+\nu+1-2 = 0. \tag{A.19}$$

Thus, the $(1+x)$ factors cancel completely. The integral reduces to

$$H(s) = \frac{sin(\nu\pi)}{\pi} \int_0^{\infty} \frac{x^{\nu-1}}{1+(1+s/\omega_l)x}\, dx. \tag{A.20}$$

Using the standard integral [49, formula 3.241.2]

$$\int_0^{\infty} \frac{x^{\alpha-1}}{1+\beta x}\, dx = \frac{\pi}{\beta^{\alpha} sin(\alpha\pi)}, \qquad 0 < \alpha < 1, \tag{A.21}$$

with $\alpha = \nu$ and $\beta = 1 + s/\omega_l$, then

$$H(s) = \frac{sin(\nu\pi)}{\pi} \cdot \frac{\pi}{sin(\nu\pi)} \cdot \frac{1}{(1+s/\omega_l)^{\nu}} = \frac{1}{(1+s/\omega_l)^{\nu}}. \tag{A.22}$$

■

A.2.3. Cole-Cole

Transfer function: $H(s) = \frac{1}{1+\left(\frac{s}{\omega_l}\right)^{\nu}}$, $0 < \nu < 1$, $\omega_l \in \mathbb{R}_+^*$.

DRT-based frequency response: $H(j\omega) = \int_0^{\infty} \frac{G(\tau)}{1+j\omega\tau}\, d\tau$.

DRT kernel: $G(\tau) = \frac{\sin(\nu\pi)}{\pi} \frac{\omega_l{}^{\nu}\tau^{\nu-1}}{1+2(\omega_l\tau)^{\nu}cos(\nu\pi)+(\omega_l\tau)^{2\nu}}$.

Proof.

For $0 < \nu < 1$, $\omega_l > 0$, set $u = \omega_l\tau$, then with $s \to j\omega$, the integral (A.7) becomes

$$H(s) = \frac{\sin(\nu\pi)}{\pi} \int_0^{\infty} \frac{u^{\nu-1}}{1+(s/\omega_l)u} \frac{du}{1+2u^{\nu}\cos(\nu\pi)+u^{2\nu}}. \tag{A.23}$$

As

$$\int_0^{\infty} \frac{x^{\alpha-1}}{(1+\beta x)(1+2x^{\alpha}\cos(\alpha\pi)+x^{2\alpha})}\, dx = \frac{\pi}{\sin(\alpha\pi)} \frac{1}{1+\beta^{\alpha}} \tag{A.24}$$

the integral can be evaluated by a change of variables and using the reflection formula for the Gamma function, or by using the residue theorem or also using [49,50] where similar integrals can be found. With $\alpha = \nu$, $\beta = s/\omega_l$, relation (A.23) becomes

$$H(s) = \frac{\sin(\nu\pi)}{\pi} \frac{\pi}{\sin(\nu\pi)} \frac{1}{1+(s/\omega_l)^{\nu}} = \frac{1}{1+(s/\omega_l)^{\nu}}. \tag{A.25}$$

■

The curve $G(\tau)$ is represented by Figure A.2 for $\omega_l = 1$ and $\nu = 0.5$. The shape of this curve is similar to the one in Figure 11.

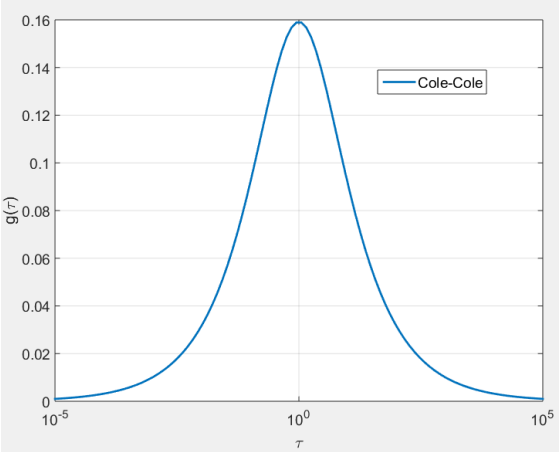

Figure A.2. Representation of kernel $G(\tau)$ of Cole-Cole transfer function.

A.2.4. Fractional band-pass

Transfer function: $H(s) = \frac{\left(\frac{s}{\omega_h}+1\right)^{\nu-1}}{\left(\frac{s}{\omega_l}+1\right)^{\nu}}$, $0 < \nu < 1$, $\omega_l \in \mathbb{R}_+^*$, $\omega_h \in \mathbb{R}_+^*$.

DRT-based frequency response: $H(j\omega) = \int_0^\infty \frac{G(\tau)}{1+j\omega\tau}\, d\tau$.

DRT kernel: $G(\tau) = \frac{\sin(\nu\pi)}{\pi} \frac{{\omega_l}^{\nu}}{{\omega_h}^{\nu-1}} \frac{(\tau\omega_h-1)^{\nu-1}}{(1-\tau\omega_l)^{\nu}}$ if $\frac{1}{\omega_h} \le \tau \le \frac{1}{\omega_l}$ else $G(\tau) = 0$.

Proof. With $0 \le \nu \le 1$, $0 < \omega_l < \omega_h$, consider the change of variable

$$u = \frac{\tau\omega_h - 1}{1 - \tau\omega_l}, \tag{A.26}$$

then u goes from 0 to ∞ as τ goes from $1/\omega_h$ to $1/\omega_l$. Solving for τ:

$$\tau = \frac{1+u}{\omega_h + u\omega_l}, \qquad d\tau = \frac{\omega_h - \omega_l}{(\omega_h + u\omega_l)^2}\, du. \tag{A.27}$$

Additionally, the following equalities hold:

$$1 - \tau\omega_l = \frac{\omega_h - \omega_l}{\omega_h + u\omega_l}, \qquad \tau\omega_h - 1 = \frac{u(\omega_h - \omega_l)}{\omega_h + u\omega_l}. \tag{A.28}$$

With $s \to j\omega$, the integral (A.7) becomes

$$\int_0^\infty \frac{G(\tau)}{1+s\tau}\, d\tau = \frac{\sin(\nu\pi)}{\pi} \frac{\omega_l^{\nu}}{\omega_h^{\nu-1}} \int_0^\infty \frac{u^{\nu-1}}{\omega_h + s + u(\omega_l + s)}\, du. \tag{A.29}$$

Using the standard integral [49, formula 3.241.2] with $\alpha = \nu$, $A = \omega_h + s$, $B = \omega_l + s$:

$$\int_0^\infty \frac{u^{\nu-1}}{A + Bu}\, du = \frac{\pi}{\sin(\nu\pi)} \frac{A^{\nu-1}}{B^{\nu}} = \frac{\omega_l^{\nu}}{\omega_h^{\nu-1}} \frac{(\omega_h + s)^{\nu-1}}{(\omega_l + s)^{\nu}}. \tag{A.30}$$

Now, factor ω_l and ω_h:

$$\frac{(\omega_h + s)^{\nu-1}}{(\omega_l + s)^{\nu}} = \frac{\omega_h^{\nu-1}(1 + s/\omega_h)^{\nu-1}}{\omega_l^{\nu}(1 + s/\omega_l)^{\nu}}. \tag{A.31}$$

Thus,

$$\int_0^{\infty} \frac{G(\tau)}{1 + s\tau}\, d\tau = \frac{\omega_l^{\nu}}{\omega_h^{\nu-1}} \cdot \frac{\omega_h^{\nu-1}}{\omega_l^{\nu}} \frac{(1 + s/\omega_h)^{\nu-1}}{(1 + s/\omega_l)^{\nu}} = \frac{(1 + s/\omega_h)^{\nu-1}}{(1 + s/\omega_l)^{\nu}}. \tag{A.32}$$

■

A.2.5. Fractional low-pass

Transfer function: $H(s) = \frac{\left(\frac{s}{\omega_h}+1\right)^{\nu}}{\left(\frac{s}{\omega_l}+1\right)^{\nu}}$ $0 < \nu < 1,\ \omega_l \in \mathbb{R}_+^*,\ \omega_h \in \mathbb{R}_+^*$.

DRT-based frequency response: $H(j\omega) = \frac{1}{s}\left(\frac{\omega_l}{\omega_h}\right)^{\nu} + \int_0^{\infty} \frac{G(\tau)}{1+j\omega\tau}\, d\tau$.

DRT kernel: $G(\tau) = \frac{\sin(\nu\pi)}{\pi}\left(\frac{\omega_l}{\omega_h}\right)^{\nu} \frac{(\tau\omega_h - 1)^{\nu}}{(1-\tau\omega_l)^{\nu}}$, if $\frac{1}{\omega_h} \le \tau \le \frac{1}{\omega_l}$ else $G(\tau) = 0$.

Proof. Using the change of variable

$$u = \frac{1 - \tau\omega_l}{\tau\omega_h - 1}, \tag{A.33}$$

then u goes from ∞ to 0 as τ goes from $1/\omega_h$ to $1/\omega_l$.

Additionally,

$$\tau = \frac{1 + u}{\omega_l + u\omega_h}, \qquad d\tau = -\frac{\omega_h - \omega_l}{(\omega_l + u\omega_h)^2}\, du, \tag{A.34}$$

and

$$1 - \tau\omega_l = \frac{u(\omega_h - \omega_l)}{\omega_l + u\omega_h}, \qquad \tau\omega_h - 1 = \frac{\omega_h - \omega_l}{\omega_l + u\omega_h}. \tag{A.35}$$

With $s \to j\omega$, Eq (A.7) becomes

$$\int_0^{\infty} \frac{G(\tau)}{1 + s\tau}\, d\tau = \frac{sin(\nu\pi)}{\pi}\left(\frac{\omega_l}{\omega_h}\right)^{\nu} (\omega_h - \omega_l) \int_0^{\infty} \frac{u^{-\nu}}{(\omega_l + u\omega_h)\big(\omega_l + s + u(\omega_h + s)\big)}\, du. \tag{A.36}$$

Using partial fraction decomposition:

$$\frac{1}{(\omega_l + u\omega_h)\big(\omega_l + s + u(\omega_h + s)\big)} = \frac{1}{s(\omega_l - \omega_h)}\left(\frac{\omega_h + s}{\omega_l + s + u(\omega_h + s)} - \frac{\omega_h}{\omega_l + u\omega_h}\right), \tag{A.37}$$

and the standard integral [49, formula 3.241.2]

$$\int_0^\infty \frac{x^{\alpha-1}}{A+Bx}\,dx = \frac{\pi}{sin(\alpha\pi)}\frac{A^{\alpha-1}}{B^\alpha}, \qquad 0<\alpha<1, \tag{A.38}$$

with $\alpha = 1-\nu$, we obtain after simplification:

$$\int_0^\infty \frac{G(\tau)}{1+s\tau}\,d\tau = \frac{(1+s/\omega_h)^\nu}{(1+s/\omega_l)^\nu} - \frac{1}{s}\left(\frac{\omega_l}{\omega_h}\right)^\nu. \tag{A.39}$$

Adding the static term $\frac{1}{s}(\omega_l/\omega_h)^\nu$ gives

$$H(s) = \frac{(1+s/\omega_h)^\nu}{(1+s/\omega_l)^\nu}. \tag{A.40}$$

■

A.2.6. Bounded fractional integrator

Transfer function: $H(s) = \frac{1}{s}\frac{\left(\frac{s}{\omega_h}+1\right)^{1-\nu}}{\left(\frac{s}{\omega_l}+1\right)^{1-\nu}}$.

DRT-based frequency response: $H(j\omega) = \frac{1}{s}\left(\frac{\omega_l}{\omega_h}\right)^\nu + \int_0^\infty \frac{G(\tau)}{1+j\omega\tau}\,d\tau$.

DRT kernel: $G(\tau) = \frac{\sin((1-\nu)\pi)}{\pi}\left(\frac{\omega_l}{\omega_h}\right)^{1-\nu}\ \frac{(1-\tau\omega_l)^\nu}{(\tau\omega_h-1)^\nu}$ if $\frac{1}{\omega_h} \le \tau \le \frac{1}{\omega_l}$ else $G(\tau) = 0$.

Proof. Using the change of variable

$$u = \frac{1-\tau\omega_l}{\tau\omega_h - 1}, \tag{A.41}$$

it is obtained

$$\tau = \frac{1+u}{\omega_l + u\omega_h}, \qquad d\tau = -\frac{\omega_h-\omega_l}{(\omega_l+u\omega_h)^2}\,du, \tag{A.42}$$

and

$$1-\tau\omega_l = \frac{u(\omega_h-\omega_l)}{\omega_l+u\omega_h}, \qquad \tau\omega_h - 1 = \frac{\omega_h-\omega_l}{\omega_l+u\omega_h}. \tag{A.43}$$

With $s \to j\omega$, Eq (A.7) becomes

$$\int_0^\infty \frac{G(\tau)}{1+s\tau}\,d\tau = \frac{sin\big((1-\nu)\pi\big)}{\pi}\left(\frac{\omega_l}{\omega_h}\right)^{1-\nu}(\omega_h - \omega_l)\int_0^\infty \frac{u^\nu}{(\omega_l+u\omega_h)\big(\omega_l+s+u(\omega_h+s)\big)}\,du. \tag{A.44}$$

Using partial fraction decomposition:

$$\frac{1}{(\omega_l + u\omega_h)\big(\omega_l + s + u(\omega_h + s)\big)} = \frac{1}{s(\omega_l - \omega_h)}\left(\frac{\omega_h + s}{\omega_l + s + u(\omega_h + s)} - \frac{\omega_h}{\omega_l + u\omega_h}\right), \tag{A.45}$$

and the standard integral [49, formula 3.241.2]

$$\int_0^\infty \frac{x^{\alpha-1}}{A + Bx}\,dx = \frac{\pi}{\sin(\alpha\pi)}\frac{A^{\alpha-1}}{B^\alpha}, 0 < \alpha < 1, \tag{A.46}$$

it is obtained after simplification:

$$\int_0^\infty \frac{G(\tau)}{1 + s\tau}d\tau = \frac{1}{s}\left[\frac{(1 + s/\omega_h)^{1-\nu}}{(1 + s/\omega_l)^{1-\nu}} - \left(\frac{\omega_l}{\omega_h}\right)^{1-\nu}\right]. \tag{A.47}$$

Adding the static term $\frac{1}{s}(\omega_l/\omega_h)^{1-\nu}$ yields:

$$H(s) = \frac{1}{s}\left[\frac{(1 + s/\omega_h)^{1-\nu}}{(1 + s/\omega_l)^{1-\nu}}\right]. \tag{A.48}$$

Finally, using the identity

$$\frac{(1 + s/\omega_l)^{1-\nu}}{(1 + s/\omega_h)^{1-\nu}} - 1 + \left(\frac{\omega_l}{\omega_h}\right)^{1-\nu} = \frac{(1 + s/\omega_h)^{1-\nu}}{(1 + s/\omega_l)^{1-\nu}}, \tag{A.49}$$

the following transfer function is obtained:

$$H(s) = \frac{1}{s}\frac{(1 + s/\omega_h)^{1-\nu}}{(1 + s/\omega_l)^{1-\nu}}. \tag{A.50}$$

■

Similarly, the following should be demonstrated the following

Transfer function: $H(s) = \frac{1}{s}\frac{\left(\frac{s}{\omega_l}+1\right)^\nu}{\left(\frac{s}{\omega_h}+1\right)^\nu}$.

DRT-based frequency response: $H(j\omega) = \frac{1}{j\omega} + \int_0^\infty \frac{G(\tau)}{1+j\omega\tau}\,d\tau$.

DRT kernel: $G(\tau) = \frac{\sin(\nu\pi)}{\pi}\left(\frac{\omega_h}{\omega_l}\right)^\nu \frac{(1-\tau\omega_l)^\nu}{(\tau\omega_h-1)^\nu}$ if $\frac{1}{\omega_h} \le \tau \le \frac{1}{\omega_l}$ else $G(\tau) = 0$.

A.2.7. Diffusion

Transfer function: $H(s) = \frac{e^{-z\sqrt{as+b}}}{\sqrt{as+b}}$ $a > 0, b > 0, z > 0$.

DRT-based frequency response: $H(j\omega) = \int_0^\infty \frac{G(\tau)}{1+j\omega\tau}\,d\tau$.

DRT kernel: $G(\tau) = \frac{z}{2\sqrt{\pi a}}\tau^{-3/2}e^{\left(-\frac{z^2}{4a\tau}-b\tau\right)}$.

Proof. For $a > 0, b > 0, z > 0$ and with $s \to j\omega$, Eq (A.7) becomes

$$H(s) = \frac{z}{2\sqrt{\pi a}} \int_0^\infty \frac{\tau^{-3/2}}{1+s\tau} e^{\left(-\frac{z^2}{4a\tau} - b\tau\right)} d\tau. \tag{A.51}$$

Using the identity [51, Eq 29.3.84]

$$\int_0^\infty \frac{x^{-3/2}}{1+sx} e^{\left(-\frac{\alpha}{x} - \beta x\right)} dx = \frac{\sqrt{\pi}}{\sqrt{\alpha}} \frac{e^{-z\sqrt{\alpha+\beta}}}{\sqrt{\alpha+\beta} + s\sqrt{\alpha}}, \tag{A.52}$$

with $\alpha = z^2/(4a)$ and $\beta = b$, then

$$H(s) = \frac{z}{2\sqrt{\pi a}} \cdot \frac{\sqrt{\pi}}{z/\left(2\sqrt{a}\right)} \cdot \frac{e^{-z\sqrt{z^2/(4a)+b}}}{\sqrt{z^2/(4a)+b} + s\, z/\left(2\sqrt{a}\right)} = \frac{e^{-z\sqrt{as+b}}}{\sqrt{as}+b}. \tag{A.53}$$

■

These various kernels are represented in Figure A.3 for $\omega_l = 0.001\ rd/s$, $\omega_h = 5000\ rd/s$, $\nu = 0.5$.

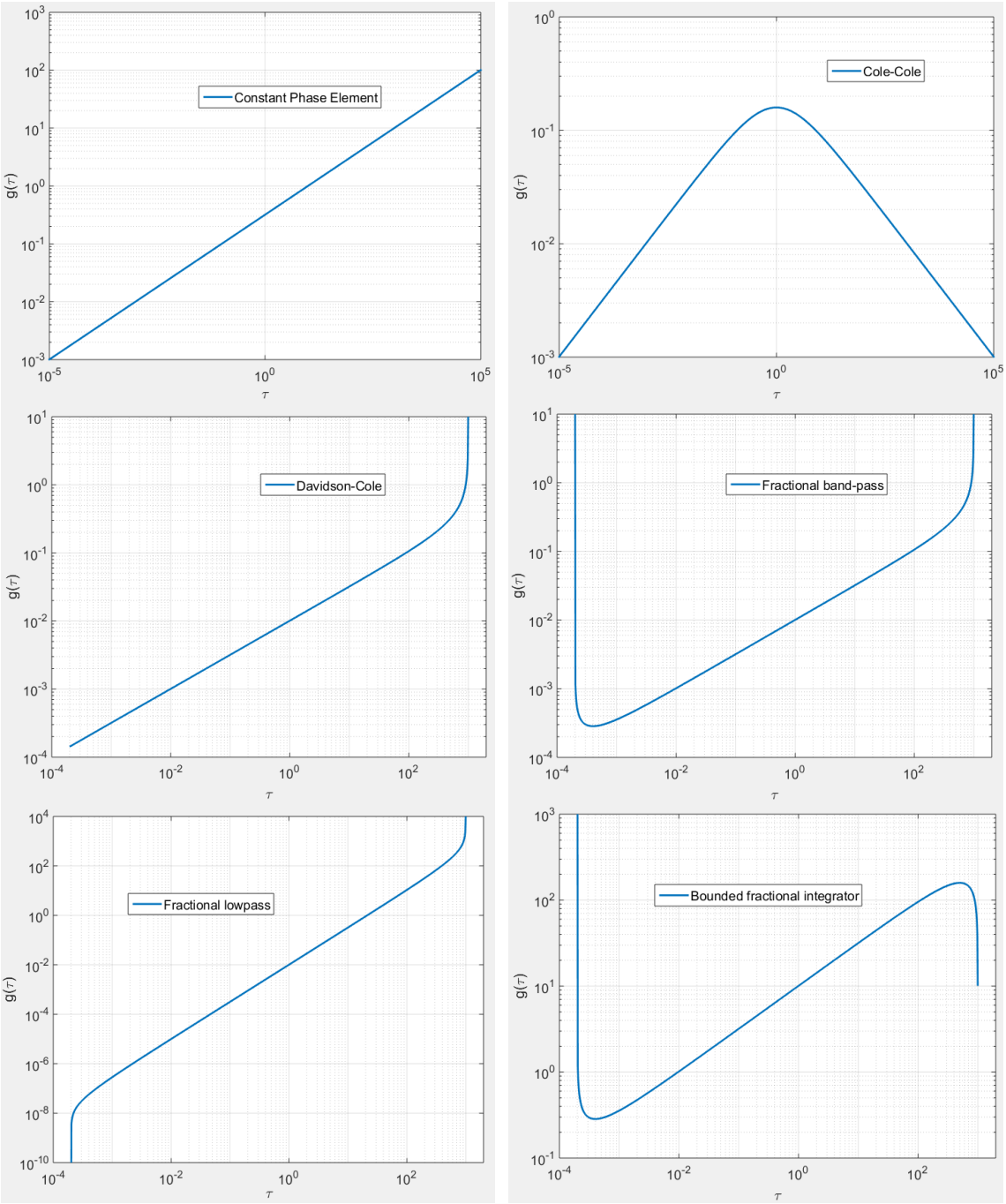

Figure A.3. Representation of kernel $G(\tau)$ proposed in Section A.2 for $\omega_l = 0.001$ rad/s, $\omega_h = 5000$ rad/s, and $\nu = 0.5$.